Albumin reprograms the B cell transcriptional landscape and improves neutrophil antimicrobial function in patients with decompensated cirrhosis

Joan Clària, Ferran Aguilar, Juan-José Lozano, Laura Jiménez-Gracia, Juan C. Nieto, Berta Romero-Grimaldo, Xavi Marcos-Fa, Emma Giarracco, Emmanuel Weiss, Jonel Trebicka, Inmaculada Hernàndez, Javier Fernandez, Mireia Casulleras, Cristina López-Vicario, Sinan Muldur, Alex Hopke, Alexandru Vlagea, Ana M. Aransay, Domenica Marchese, Mauro Bernardi, Rajiv Jalan, Paolo Angeli, Giuliana Magri, Andrea Cerutti, Daniel Irimia, Holger Heyn, Vicente Arroyo, Richard Moreau

Table of contents

Supplementary methods

Selection of Patients from the PREDICT Study

The PREDICT study was a large-scale prospective observational multicenter investigation aimed to identify precipitants and short-term (3-month) clinical course phenotypes in patients hospitalized for acutely decompensated (AD) cirrhosis without acute-on-chronic liver failure (ACLF) (*1*). AD cirrhosis was defined by the acute development of ascites, encephalopathy and/or gastrointestinal hemorrhage (*1*), according to previous studies (*2,3*). AD cirrhosis develops in the context of intense systemic inflammation (*2-5*). ACLF is the extreme expression of AD cirrhosis and is characterized by extrahepatic organ failure(s) and high short-term mortality (*2,3*). The PREDICT study consisted of a prespecified longitudinal collection of clinical and standard laboratory data and biological samples, including whole-blood for RNA-seq. Investigators used an electronic clinical-report form to report clinical data, including treatments and standard laboratory data (*1*). Data were continuously monitored on-line by the Data Management Center of the European Foundation for the Study of Chronic Liver Failure. Among patients of the PREDICT study, three distinct clinical phenotypes were identified according to the clinical course. Approximately 20% of the patients had pre-ACLF at enrollment because these patients developed ACLF within 3 months. It was the group with the highest grade of systemic inflammation at enrollment. The other two clinical phenotypes (unstable and stable decompensated cirrhosis) included patients with lower grade of systemic inflammation, which may rapidly improve under standard medical therapy (*1*). Unfortunately, among patients admitted for AD cirrhosis without ACLF, there are currently no available markers enabling to distinguish those who will develop ACLF from those who will not develop this complication (1). Therefore, it is currently not possible to design studies, interventional, in which the inclusion criterion would be the presence of AD cirrhosis at imminent risk of ACLF. For this reason, prospective observational studies are of most interest in the assessment of

treatments in these patients.

The selection of patients from PREDICT followed this criteria: i) all AD patients were at imminent risk of ACLF at enrollment (T1) and developed ACLF during the index hospitalization (T2); ii) in all patients, bulk blood RNA-seq data were obtained at T1 and T2; iii) None of the forty-nine patients had received albumin before T1; iv) Thirty out of the forty-nine patients had received albumin between T1 and T2 and composed the albumin group whereas the nineteen others remained free of albumin between T1 and T2 and composed the non-albumin group. In the albumin group, the median time between T1 and T2 for blood collections for RNA-seq was 11.5 days (interquartile range [IQR], 6.2-18.7). The median duration of HSA treatment was 2.5 days (IQR, 2-6) and the dose was 40.0 g per day (IQR, 22.5-57.5). The time between the last HSA administration and subsequent blood collection was 1.5 days (IQR, 0.0-2.7), indicating that we explored patients soon after HSA administration. In the non-albumin group, the median time between T1 and T2 was 29 days (IQR, 16-52). The 60 first patients with AD cirrhosis and imminent risk of ACLF enrolled in the PREDICT study were eligible. Of these, 11 (9 who had received albumin prior baseline transcriptomics and 2 showing poor-quality control in the transcriptomic analysis) were excluded. The *in vivo* study was therefore performed in 49 patients. The electronic case-reports form of the PREDICT study prespecified the following indications for intravenous albumin: large-volume therapeutic paracentesis, spontaneous bacterial peritonitis, hepatorenal syndrome-acute kidney injury, and other indication. Among the 30 patients who had received intravenous albumin between enrollment and ACLF development and were analyzed in the present study (**Fig. S11A**), the primary indications for albumin were large-volume therapeutic paracentesis, spontaneous bacterial peritonitis, and hepatorenal syndrome-acute kidney injury (HRS-AKI, formerly type 1 hepatorenal syndrome).

Immunophenotyping

Extended phenotyping of blood immune cells was performed by flow cytometry using the following panels of antibodies (clones are indicated within brackets): TBNK panel including CD4 (SK3), CD56 (MY31), CD8 (RPA-T8), CD16 (3G8), CD14, CD45 (2D1), CD3 (SP34-2) and CD19 (SJ25C1); B cell panel including CD21 (B-ly4), IgD (IA6-2), CD24 (ML5), CD38 (HIT2), CD27 (M-T271), CD45 (2D1), IgM (G20-127) and CD19 (SJ25C1); dendritic cell panel including CD3 (SK7), CD16 (3G8), CD19 (SJ25C1), CD20 (L27), CD14 (MφP9), CD56 (NCAM16.2), CD1c (F10), CD123 (7G3), CD11c (B-ly6), CD34 (8G12) + CD117 (YB5.B8), CD45 (2D1), HLA-DR (L243) and CD141 (1A4); and T regulatory cell panel including HLA-DR (L243), CD25 (M-A251), CD127 (HIL-7R-M21), CD45RO (UCHL1), CD3 (SK7), CD4 (L200) and CCR4 (1G1). All antibodies were purchased at BD Biosciences (San Jose, CA). For immunophenotyping, the antibodies were titrated and used to stain 100 µL of EDTA-collected whole blood during 20 minutes in the dark. Then erythrocytes were lysed by incubating 20 minutes with BD FACS™ lysing solution and washed twice. After lysis, the cells were resuspended in phosphate-buffered saline. After compensation, data acquisition was performed with a BD FACSCanto II flow cytometer (Becton Dickinson, Franklin Lakes, NJ). For analysis BD FACSDiva (Becton Dickinson) software was used. A minimum of 100,000 total events were acquired. The graphical layout was created using the FlowJo software (Becton Dickinson).

Immunophenotyping and isolation of PBMCs

To assess changes in B cell phenotypes induced by albumin, PBMCs from ten healthy subjects were isolated and seeded at a density of $3x10^6$ cells/ml in RPMI 1640 medium with BAFF (Enzo Life Sciences, Farmingdale, NY) (10 ng/ml) as a survival factor, with or without albumin (15 mg/ml) and incubated at 37ºC, 5% CO_2 for 24 hours. At the end of the incubation period, cells were centrifuged at 400 g for 5 min and resuspended in cold DPBS. Then, cells were incubated for 30 min with the LIVE/DEAD yellow viability marker (L34959, Thermo Fisher

Scientific), and washed with PBS. Thereafter, cells were stained in MACS buffer (pH 7.4) for 20 min with the following anti-human antibodies:

Antigen	Isotype	Conjugated dye	Reference	Company
CD10	Mouse IgG1, κ	BV421	312217	Biolegend (San Diego, CA)
CD19	Mouse IgG1, κ	Pacific Blue	302224	Biolegend
CD24	Mouse IgG2a, κ	PE-Cy7	311120	Biolegend
CD27	Mouse IgG1, κ	BV650	302827	Biolegend
CD38	Mouse IgG1, κ	APC-Fire810	CUSTOM	Biolegend
IgD	Goat F(ab')2 IgG	FITC	2032-02	Southern Biotech (Birmingham, AL)

After washing with PBS, the cells were fixed with paraformaldehyde at 4% for 12 min and then washed again with PBS. Finally, cells were resuspended in 250 µl of cold PBS. The analysis was performed on a Cytek Aurora spectral flow cytometer (Cytek Biosciences, Fremont, CA).

PBMC and neutrophil isolation

Peripheral venous blood (20 ml) was obtained by venipuncture and collected into EDTA-coated, sterile, pyrogen-free tubes (Becton Dickinson). Blood samples were centrifuged at 200 g for 10 min and sedimented cells were diluted with DPBS without calcium and magnesium ($DPBS^{--}$) up to a volume of 20 ml. Diluted blood was layered over 13.3 ml of Ficoll-Hypaque and centrifuged at 500 g for 25 min with the break-off. PBMCs obtained from the mononuclear cell layer were then incubated with pre-warmed ammonium-chloride-potassium lysis buffer for 10 min at room temperature to remove red blood cells and then centrifuged at 400 g for 5 min. The resultant pellet was washed with $DPBS^{--}$. Isolated PBMCs were re-suspended in RPMI 1640 medium containing penicillin (100 U/ml), streptomycin (100 U/ml), and L-glutamine (4 mM) without fetal bovine serum (FBS) and viable cells were then automatically counted. After 30 minutes of resting, $3x10^6$ viable cells were incubated at 37°C and used for bulk and scRNA-seq. Neutrophils were also isolated using the Ficoll-Hypaque method described above. Briefly,

after separation of the PBMC layer in the supernatant, neutrophils were collected from the pellet and incubated with pre-warmed ammonium-chloride-potassium lysis buffer for 10 min at room temperature to remove red blood cells and then centrifuged at 400 g for 5 min. The red blood lysis procedure was repeated twice, and the resultant pellet was washed with $DPBS^{--}$. Isolated neutrophils were resuspended in RPMI 1640 medium containing penicillin, streptomycin, and L-glutamine without FBS and used in the assays. For the chemotaxis and swarming assays, blood samples from healthy donors were purchased from RBC components (Alston, MA) and neutrophils were isolated from the blood using the STEMCELL direct neutrophil isolation kit (Vancouver, Canada), according to the manufacturer's protocols. Isolated neutrophils were counted and re-suspended in Iscove's Modified Dulbecco's Medium (IMDM).

scRNA-seq in PBMCs

PBMCs were seeded in RPMI 1640 medium at a density of $1.5x10^6$ cells/ml and incubated with either human serum albumin (Albutein®) (15 mg/ml) or vehicle (culture medium) for two hours at 37ºC in a 5% CO_2 incubator. At the end of the incubation period, cells were rapidly (within 30 min) transferred on ice to the Single Cell Genomics platform from the CNAG. PBMCs were centrifuged for 5 min at 500 g at 4°C. The supernatant was removed, and the pellet was re-suspended in 1xPBS supplemented with 0.05% BSA. Samples were filtered with a 40-µm strainer (pluriSelect) and cell concentration and viability were verified by counting with a TC20™ Automated Cell Counter (Bio-Rad Laboratories, Hercules, CA). PBMC samples from two patients and two healthy subjects were directly used for cell partition into Gel Bead in Emulsion with a Target Cell Recovery of 5,000 cells each. For all the other cases, donor matched albumin or vehicle samples were labeled by cell hashing and pooled in one 10x Genomics channel to avoid technical biases. Cell hashing was performed following the manufacturer's instructions (Cell hashing and Single Cell Proteogenomics Protocol Using

TotalSeq™ Antibodies; BioLegend, San Diego, CA). Briefly, for each sample, 1-2 million cells were re-suspended in 100 µl of Cell Staining Buffer (BioLegend) and incubated for 10 min at 4ºC with 5 µl of Human TruStain FcX™ Fc Blocking reagent (BioLegend). Next, a specific TotalSeq-A antibody-oligo conjugate (anti-human Hashtag 1-4, Biolegend) was added to each of the two conditions (albumin and vehicle) and incubated on ice for 30 min. Cells were then washed three times with cold PBS-0.05% BSA and centrifuged for 5 min at 500 g at 4°C. Finally, cells were re-suspended in an appropriate volume of 1xPBS-0.05% BSA to obtain a final cell concentration 500-1000 cells/µl, suitable for 10x Genomics scRNA-seq. An equal volume of hashed cell suspension from each of the two conditions was mixed and filtered with a 40-µm strainer. Cell concentration was verified by counting with a TC20™ Automated Cell Counter. Then, cells were partitioned into Gel Bead In Emulsions with a Target Cell Recovery of 10,000 total cells. Sequencing libraries were prepared using the v3.0 single-cell 3' mRNA kit (10x Genomics, Pleasanton, CA) with some adaptations for cell hashing, as indicated in TotalSeq™-A Antibodies and Cell Hashing with 10x Single Cell 3' Reagent Kit v3 Protocol from BioLegend. Briefly, 1 µl of 0.2 µM hashtag oligonucleotide (HTO) primer (GTGACTGGAGTTCAGACGTGTGC*T*C; *phosphorothioate bond) was added to the cDNA amplification reaction to amplify the hashtag oligos together with the full-length cDNAs. A SPRI selection clean-up was performed to separate mRNA-derived cDNA (>300 bp) from antibody-oligo-derived cDNA (<180 bp), as described in the above-mentioned protocol. 10x Genomics cDNA libraries were prepared following the 10x Genomics Single Cell 3' mRNA kit protocol, while HTO cDNAs were indexed by PCR as follows. Briefly, 5 µl of purified hashtag oligo cDNA were mixed with 2.5 µl of 10 µM Illumina TruSeq D70X_s primer (IDT) carrying a different i7 index for each sample, 2.5 µl of SI primer from 10x Genomics Single Cell 3' mRNA kit, 50 µl of 2xKAPA HiFi PCR Master Mix (KAPA Biosystem) and 40 µl of nuclease-free water. The reaction was carried out using the following thermal cycling

conditions: 98°C for 2 min (initial denaturation), 12 cycles of 98°C for 20 sec, 64°C for 30 sec, 72°C for 20 sec, and a final extension at 72°C for 5 min. The HTO libraries were purified with 1.2X SPRI bead selection. Size distribution and concentration of cDNA and HTO libraries were verified on an Agilent Bioanalyzer High Sensitivity chip (Agilent Technologies, Santa Clara, CA). Finally, sequencing of HTO and cDNA libraries was carried out on a NovaSeq6000 system (Illumina Inc., San Diego, CA) to obtain approximately >25,000 reads per cell.

Data processing of scRNA-seq.

To profile the cellular transcriptome, we processed the sequencing reads using the CellRanger software package (version 6.1.1) from 10X Genomics Inc. We mapped the reads against the human GRCh38 reference genome. For the libraries where multiple samples were pooled together, we also specified the HTO associated to each sample. All analyses presented in this manuscript were conducted using R version 4.0.5, along with specific analysis and data visualization packages such as Seurat R package (version 4.0.0) (*6*) SeuratObject package (version 4.0.1), and other packages specified in the subsequent sections. All plots were generated using ggplot2 package (version 3.3.3). For sample demultiplexing, we demultiplexed cell hashtags as described in Stoeckius et al. (*7*) for each library separately. Briefly, we normalized HTO counts using a centered log ratio and run "HTODemux()" function from Seurat package with the default parameters. Each barcode was classified to its sample-of-origin, and multiplets (barcodes assigned to more than one condition) or negatives (barcodes not assigned to any condition) were discarded for downstream analysis. For quality control (QC) and cell annotation, we ensured that there were no remarkable differences on the main QC metrics (library size, library complexity, percentage of mitochondrial and ribosomal expression) among the different hashed and non-hashed libraries, and then performed common QC, normalization and further analysis following the guidelines provided by Leucken et al. (*8)*.

We removed low-quality cells by filtering out barcodes with a very low number of Unique Molecular Identifiers (UMIs) (500) and genes (<250), or with a high percentage of mitochondrial expression (>20%), as it is indicative of lysed cells. Additionally, we considered removing barcodes with a large library size (>50,000) and complexity (>6,000) as they could be putative doublets. We eliminated genes that were detected in very few cells (<10). Finally, filtered data were normalized, log transformed and shared 3,000 highly variable features were used to compute Principal Component Analysis. To achieve successful cell-type annotation combining data from different donors and treatments, we removed the batch-effect with the Harmony integration method (*9*) using the library as a confounder variable. After integration, we created a k-nearest neighbors graph with the "FindNeighbors" function using the first 20 Principal Components, followed by the cell clustering with the Louvain clustering algorithm using the "FindClusters" function at different resolutions. To visualize scRNA-seq data in two-dimensional embedding, we run the Uniform Manifold Approximation and Projection algorithm. To obtain a fine-grained cell type annotation, we followed a top-down approach; first, cells were clustered into large clusters representing cell lineages (B lymphocytes, myeloid cells, T lymphocytes and NK cells), subsequently, cells from the lineages of interest were re-processed and clustered, or even sub-clustered, to define cell types and cell states. To annotate the clusters into specific cell types, we performed a Differential Expression Analysis (DEA) for all clusters to determine their marker genes using the normalized RNA counts, we examined the expression of canonical gene markers, and referred to gene markers from published annotated datasets. Low quality clusters based on poor QC metrics or platelet complexes showing dual gene markers were removed. We performed DEA for cell annotation using the Seurat function "FindMarkers" with the Wilcoxon signed-rank sum test. We defined genes to be relevant markers if the Log2 Fold Change (Log2FC) >0.25, with a FDR adjusted p-value <0.05, and if they were present in at least 25% of cells. For cell type compositional analysis and

to estimate changes in the proportions of cell types due to albumin treatment, we compared the fraction of cell types relative to all cells within each lineage population, and computed a paired Wilcoxon signed-rank sum test for each cell type comparing albumin with vehicle treated samples for AD patients and healthy donors, independently. To validate the albumin effect on CD4 T cells using scRNA-seq data, we downloaded the list of genes associated with the BTM of interest and computed a signature-specific score for each cell using the Ucell package (*10*). The BTM signature score was then assessed on specific cell populations across treatment conditions. Statistical analysis between albumin and vehicle treatment conditions was performed using a paired Wilcoxon signed-rank sum test. The code to reproduce the full analysis is hosted at Github: https://github.com/LJimenezGracia/AD-ACLF_cirrhosis_HSAtreatment.

Bulk whole blood RNA-seq.

RNA was isolated from blood stored in Tempus tubes using the Tempus™ Spin RNA Isolation Kit (Applied Biosystems, Foster City, CA) as previously described (*5*). RNA quality was assessed using Agilent RNA 6000 Nano and Pico Chips (Agilent Technologies) and concentration via Qubit RNA HS Assay Kit (Thermo Fisher Scientific). Sequencing libraries were prepared using the TruSeq Stranded Total RNA with Ribo-Zero Globin kit and TruSeq RNA CD Index Plate (both from Illumina Inc.) following TruSeq Stranded Total RNA Sample Prep-guide (Part # 15031048 Rev. E). Starting from 500 ng of total RNA, rRNA and globin mRNA were depleted, and remaining RNA was purified, fragmented, and primed for cDNA synthesis. cDNA first strand was synthesized with SuperScript-II Reverse Transcriptase (Thermo Fisher Scientific, Waltham, MA) for 10 min at 25°C, 15 min at 42°C, 15 min at 70°C and pause at 4°C. cDNA second strand was synthesized with Illumina reagents at 16°C for 1 hour. Then, A-tailing and adaptor ligation were performed. Finally, enrichment of libraries was

achieved by PCR (30 s at 98°C; 15 cycles of 10 s at 98°C, 30 s at 60°C, 30 s at 72°C; 5 min at 72°C and pause at 4°C). Afterwards, libraries were visualized on an Agilent 2100 Bioanalyzer using Agilent High Sensitivity DNA kit (Agilent Technologies), quantified using Qubit dsDNA HS DNA Kit (Thermo Fisher Scientific) and sequenced in a NovaSeq-6000 (Illumina Inc.) by at least 100 million paired-end 100nt reads. The reads were aligned to the hg38 genome assembly and the transcriptome using STAR v2.5.3a6 and GENCODE 26 annotation (*11*). RNA-Seq by Expectation Maximization (RSEM) v1.3.0REF.8 was used to compute the expected read counts of each sample from the corresponding binary alignment map (known as BAM) files. Trimmed mean of M values normalization method and limma-voom transformation from rounded expected counts were used to normalize the nonbiological variability. Using the HUGO Genome Nomenclature Committee, which is a resource for approved human gene nomenclature, we included protein-coding genes, and among other gene locus types, immunoglobulin genes, and T-cell receptor genes, resulting in a total of 14,520 genes for analysis. Genes brought by sexual chromosomes and mitochondrial DNA were not included in the analysis. Differential expression between groups was assessed using the moderated t-statistic (*12*).

Data processing of bulk blood RNA-seq.

Bulk blood RNA-Seq data were used for different purposes, that are listed below. RNA-seq data have been deposited at the Gene Expression Omnibus (GEO accession number, GSE171741).

Assessing differential gene expression. DEGs were defined by the simultaneous presence of two criteria, i.e., an absolute FC greater than 1.5 and moderated P value of less than 0.05.

Analyzing gene-set enrichment. The QuSAGE method, as implemented in the QuSAGE package *(13)*, was used to conduct Gene Set Enrichment Analysis (GSEA) using the 346 blood

transcription modules (BTMs) as gene sets. BTMs are gene sets related to blood cells (e.g., plasma cells, immunoglobulins (M156.1)) developed through large-scale network integration of publicly available human blood transcriptomes (*14)*. QuSAGE provides an activity score for each gene set in each pairwise comparison. A BTM was identified as DE when the QuSAGE activity score of this BTM had a False Discovery Rate (FDR) <0.05 or P <0.05, where appropriate.

Analyzing shared genes and shared BTMs. A DEG or a differentially expressed BTM was defined as shared between two comparisons when the DEG or differentially expressed BTM were concordant in sign.

Assessing immune-cell signatures with the use of SingleR software. The SingleR software (*15)* was used to compare bulk blood RNA-seq data from our study participants with a reference dataset containing 114 human bulk RNA-seq samples of sorted immune-cell populations from 4 HS (GSE107011) *(16)*. This reference dataset contained 114 human RNA-seq samples annotated to 10 main immune-cell types, including neutrophils, basophils, monocytes, dendritic cells, T cells, CD4 T cells, CD8 T cells, progenitors, B cells, and NK cells. The GSE107011 dataset also contained samples that were additionally annotated to 29 fine immune-cell types, including low-density neutrophils, low-density basophils, classical monocytes, intermediate monocytes, nonclassical monocytes, plasmacytoid dendritic cells, myeloid dendritic cells, naïve CD8 T cells, central memory CD8 T cells, effector memory CD8 T cells, terminal effector CD8 T cells, naïve CD4 T cells, Th1 cells, Th1/Th17 cells, Th17 cells, Th2 cells, T regulatory cells, follicular helper T cells, terminal effector CD4 T cells, Vd2 gamma delta T cells, non-Vd2 gamma delta T cells, MAIT cells, progenitor cells, naïve B cells, non-switched memory B cells, switched memory B cells, exhausted B cells, plasmablasts, and NK cells. The SingleR pipeline compared our bulk blood RNA-seq data, first with the 10 main immune-cell types of reference and then with the 29-fine immune-cell types. In brief, the annotation in SingleR was performed

for each whole blood transcriptome independently. The first step was to identify variable genes among each reference immune-cell types. Variable genes were defined as the top N genes that had a higher median expression in a cell-type compared to each other cell-type; here we used 70 variable genes per cell-type for the first round of analysis. Using only variable genes increased the ability to distinguish closely related cell-types. Then, a Spearman coefficient was calculated for whole blood RNA expression with each of the samples in the reference dataset. The correlation analysis was performed only on variable genes in the reference dataset. Next, multiple correlation coefficients per sample according to the named annotations of the reference dataset were aggregated to provide a single value per cell-type per sample. Of note, SingleR uses the 80^{th} percentile of correlation values, to prevent misclassification due to heterogeneity in the reference samples. Finally, in the fine-tuning step, SingleR reran the correlation analysis, but only for the top cell-types from the previous step. The lowest value cell-type was removed (or values more than 0.05 below the top value), and then this step was repeated until only two cell-types remained. The cell-type corresponding to the top value after the last run was assigned to the blood sample.

Bulk RNA-seq and real-time PCR in PBMCs

Isolation of total RNA from PBMCs was performed using the TRIzol reagent following the manufacturer's instructions. RNA concentrations were assessed in Microvolume UV-Vis Spectrophotometer (Nanodrop One, Thermo Fisher Scientific). Bulk RNA-seq was performed as described above. For real-time PCR analysis, cDNA synthesis from 500 ng of total RNA was performed using the High-Capacity cDNA Archive Kit (Applied Biosystems, Foster City, CA). Real-time PCR analysis of human IGHA1 (Hs00733892_m1, encoding IgA1), IGHM (Hs00941538_g1, encoding IgM) and IHG2 (Hs00390545_3, customized, encoding IgG2) was

performed in QuantStudio™ 7 Pro Real-Time PCR System (Thermo Fisher Scientific) using RPS18 (Hs01375212_g1, encoding for RPS18) as endogenous control.

Neutrophil degranulation assay.

After 30 minutes of resting, neutrophils were seeded at a density of $3x10^6$ cells/mL and incubated with either HSA, recombinant human albumin (both at 15 mg/ml) or vehicle control in the absence or presence of phorbol 12-myristate 13-acetate (100 nM) for 2 hours at 37ºC in a 5% CO_2 incubator. At the end of the incubation period, supernatants were collected to measure degranulation using the Neutrophil MPO Activity Assay Kit (Cayman Chemical, Ann Arbor, MI). Briefly, 25 µl of neutrophil supernatant together with 25 µl of assay buffer were added to each well of the experimental plate. Then, 50 µl of 3,3',5,5'-tetramethylbenzidine (TMB), a substrate for horseradish peroxidase, were added to each well and absorbance was measured at minute one and minute five after the addition of TMB in a microplate reader (Infinite M PLEX Monochromator, TECAN, Männedorf, Switzerland). The assay was performed at room temperature.

Neutrophil phagocytosis assay.

After 30 minutes of resting, neutrophils were seeded at a density of $5x10^5$ cells/mL and incubated with either HSA, recombinant human albumin (both at 15 mg/ml) or vehicle control for 2 hours at 37ºC in a 5% CO_2 incubator. Thereafter, 50 µL of opsonized fluorescein conjugate zymosan bioparticles or fluorescent-labeled *E. coli* (Thermo Fisher Scientific) were added to each well (ratio cells/bioparticles, 1:10) to a final volume of 200 µL and incubated at 37ºC for 60 min. Cells were then washed with sterile $DPBS^{--}$ and 100 µL trypan blue solution (diluted 1/10 in sterile $DPBS^{--}$) were added to quench fluorescence of extracellular bioparticles. Plates were finally centrifuged for 5 min at 400 g at room temperature and excess trypan blue was

carefully aspirated. The fluorescent intensity of each well was read in a microplate reader (FLUOstar Optima, Ortenberg, Germany).

Neutrophil chemotaxis assay.

A chemotaxis-phagocytosis assay in microfluidic arenas (*17*) was used to test the role of albumin on the ability of neutrophils to migrate directionally towards and to phagocytose *Candida albicans* yeast. For this purpose, microfluidic arenas were fabricated in PDMS and glass at the BioMEMS Core. The arenas were primed with a suspension of *Candida* yeast at 107 yeast cells/ml. The channels outside the arenas were washed with media to remove any extra *Candida* outside the arenas. After the addition of neutrophils to the chemotaxis assay in the presence or absence of HSA, images of the arenas were recorded on a Nikon Ti-E microscope with a motorized stage and environmental chamber. The number of neutrophils recruited to each arena was counted form brightfield images over time. The total area of GFP-expressing *Candida* was quantified from fluorescence images.

Swarming assay.

A swarming assay was used to test the contribution of HSA to the ability of neutrophils from patients to contain the growth of *Candida* clusters. To this purpose, arrays of *Candida*-adherent spots (200 μm diameter) were printed utilizing a microarray printing platform (Picospotter PolyPico, Galway, Ireland) and a solution of poly-l-lysine (Sigma-Aldrich). The arrays were printed onto ultra-clean glass slides (Thermo Fisher Scientific). The printed slides were mounted into 16-well ProPlate wells (Grace Bio-labs, Bend, OR) and 50 μL of a suspension of *Candida* inoculums in PBS were added to each well and incubated with rocking for 5 min. Following incubation, the wells were washed with PBS to remove unbound yeast from the glass surface. The mounted slides were checked to ensure appropriate patterning of targets onto the

spots with minimal non-specific binding before use. Isolated neutrophils were counted and re-suspended in IMDM + 20% FBS with the indicated concentration of albumin or vehicle, and then added to swarming chambers at 500,000 cells per well. Swarming was observed using a Nikon Ti-E microscope. Time-lapse imaging was conducted using a 10x Plan Fluor Ph1 DLL (NA=0.3) lens and endpoint images were taken with a 2x Plan Apo (NA=0.10) lens. All selected points were optimized for perfect focus before launching the experiment. Fungal growth area analysis was automated in ImageJ software.

Supplementary figures

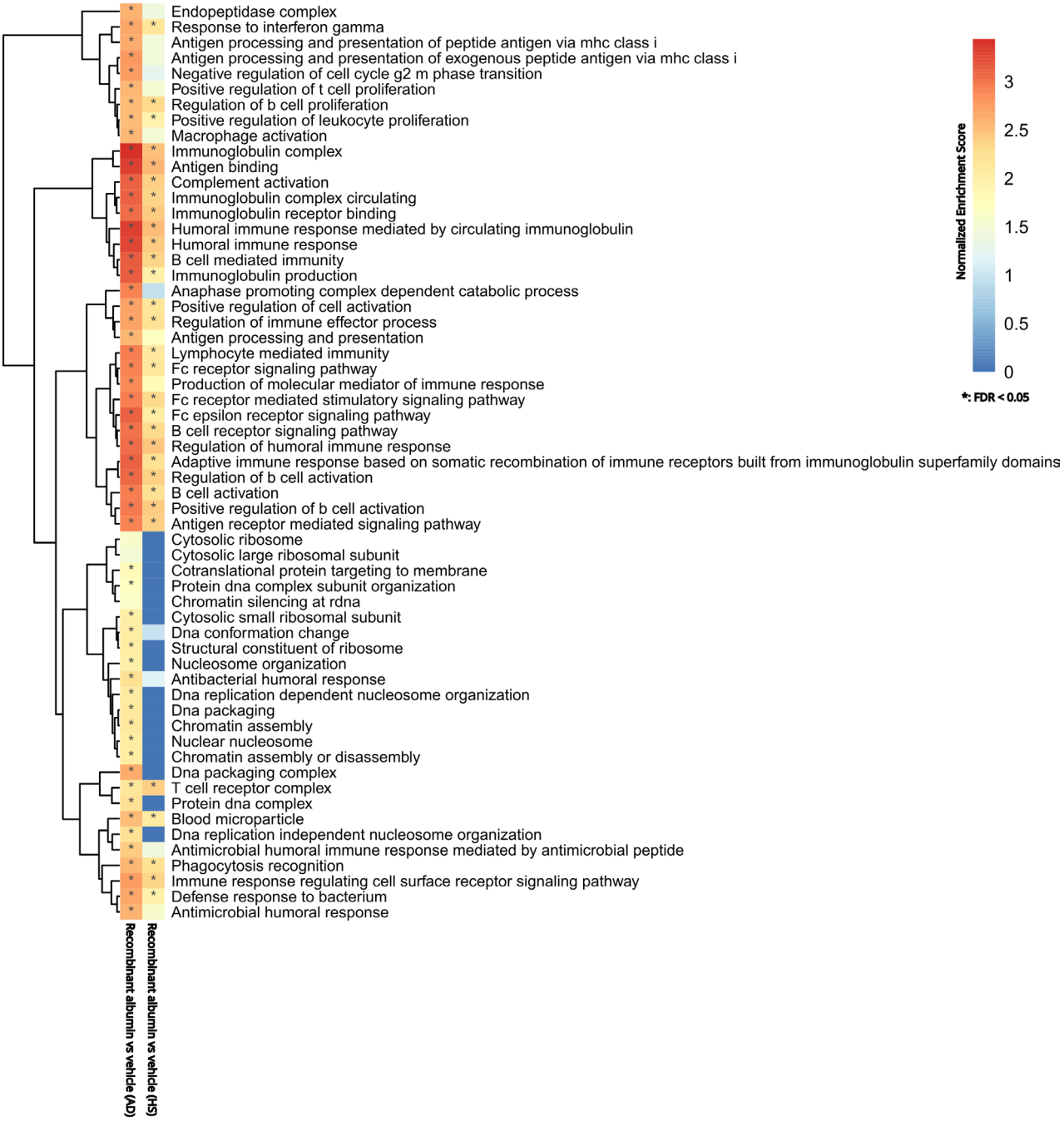

Fig. S1. **Changes in the transcriptional landscape of PBMCs isolated from HS incubated in vitro with recombinant albumin.** RNA-seq data were submitted to GSEA to generate ranked lists of genes for the following pairwise comparisons: recombinant albumin versus vehicle in PBMCs from patients with AD cirrhosis and recombinant albumin versus vehicle in PBMCs from healthy subjects. Gene-enrichment analysis was then performed. Color gradient corresponds to increasing values of the normalized enrichment score (NES) of gene sets from the less upregulated (in blue) to the most upregulated (in red). The presence of stars in cells of the heat map indicates a false discovery rate (FDR) <0.05. For comparison, the transcriptional changes in PBMCs isolated from patients with AD cirrhosis incubated *in vitro* with recombinant albumin are shown.

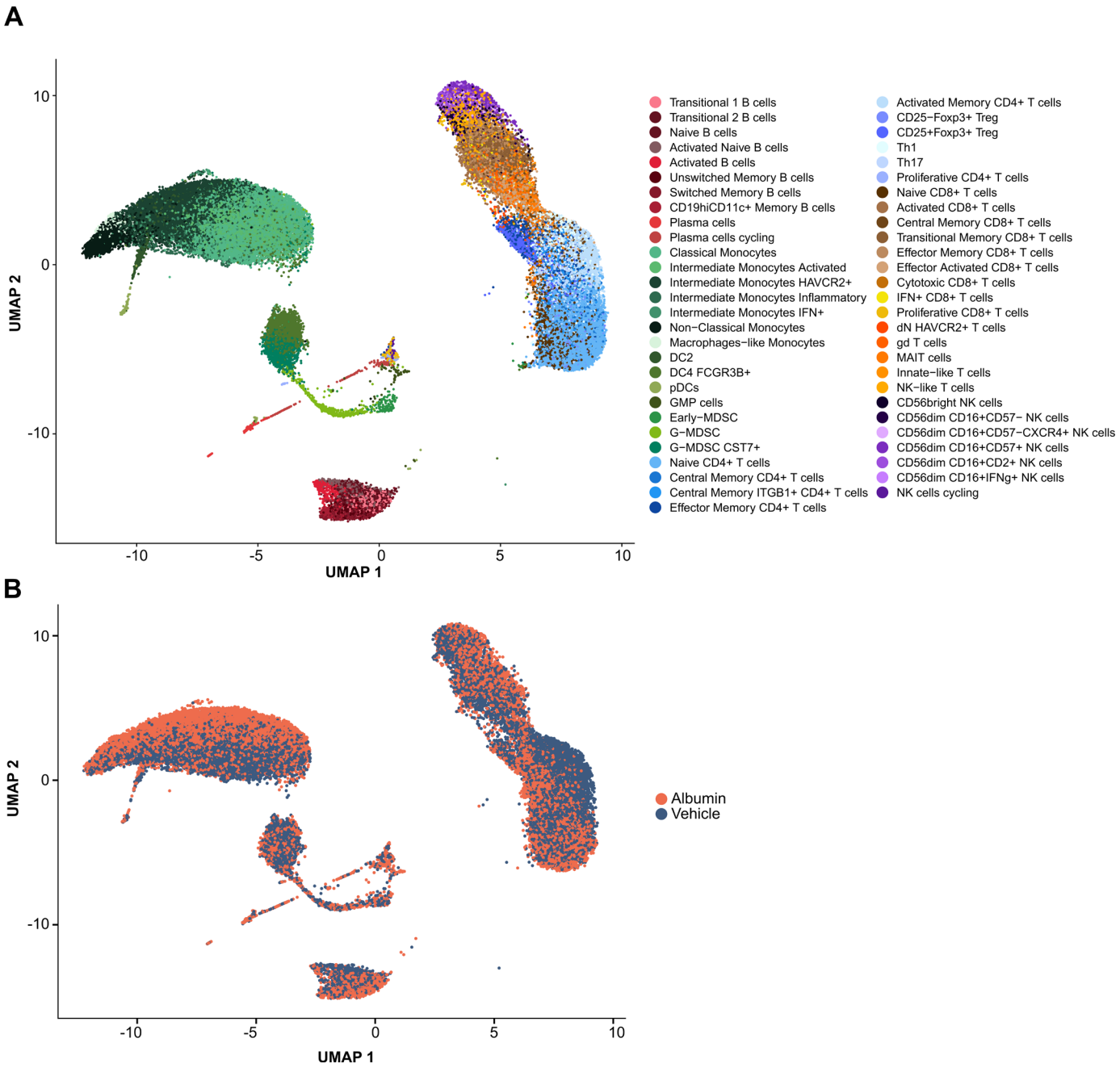

Fig. S2. Overview of results of scRNA-seq experiments of PBMCs from patients with AD cirrhosis. Fresh PBMCs from 9 patients with AD cirrhosis were exposed *in vitro* to albumin (15 mg/ml) or vehicle during two hours before performing scRNA-seq. (A) Uniform manifold approximation and projection (UMAP) of 69,293 human PBMCs from AD patients exposed to albumin and vehicle, colored by cell types (a total of 66,064 PBMCs were further analyzed after excluding NK cells). (B) Overlay of albumin and vehicle exposure on the full PBMC UMAP.

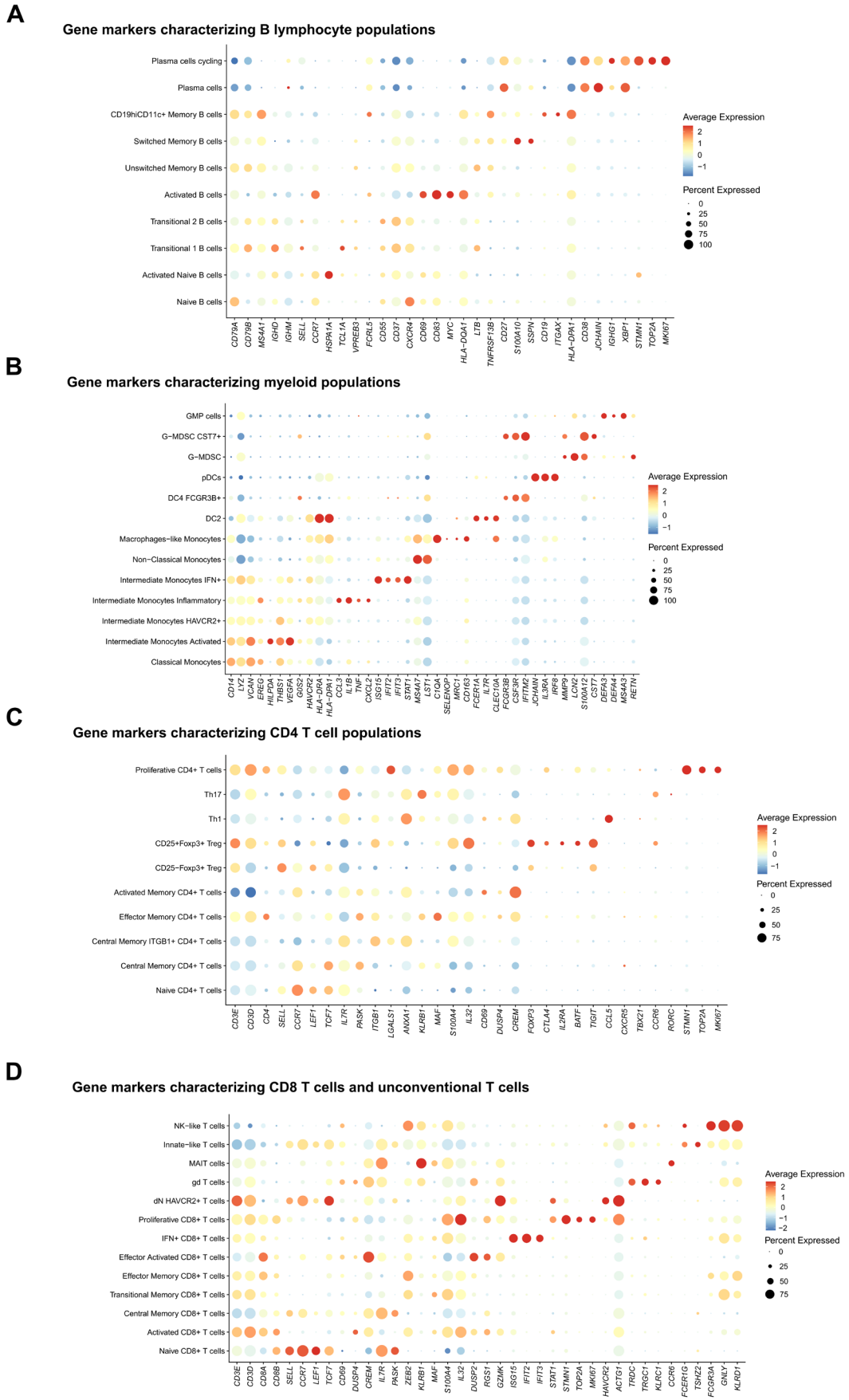

Fig. S3. Top gene markers describing all the immune-cell populations identified in the scRNA-seq dataset. Dot plot showing the average expression for top genes (*x-axis*) across all cell populations (*y-axis*) for B lymphocytes (A), myeloid cells (B), $CD4^+$ (C) and $CD8^+$ and unconventional T cells (D). Dot size represents the percentage of cells in a cluster expressing each gene, and the color indicates the average expression level.

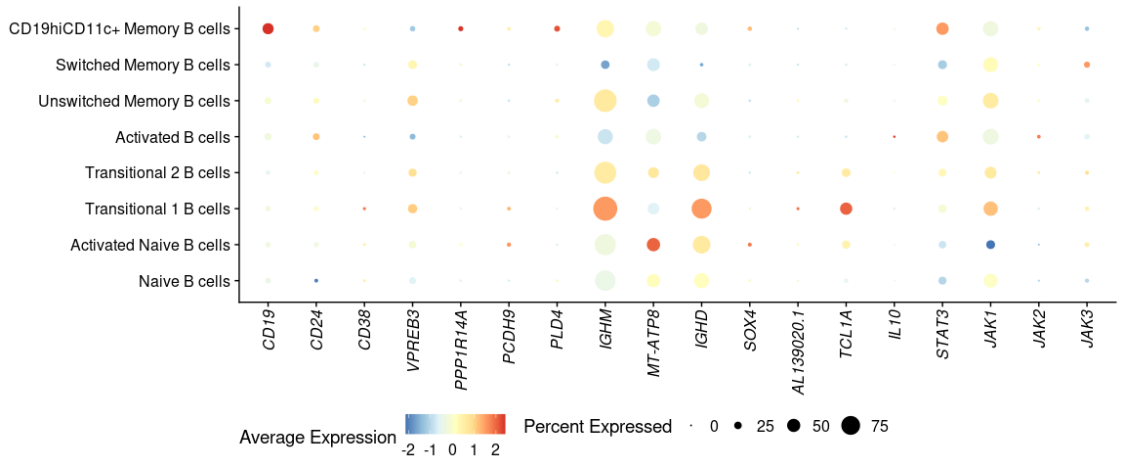

Fig. S4. Identity of the B cell populations affected by albumin using scRNA-seq data. Expression of genes associated with transitional-like identity from Steward et al. *(18)* across B cell populations, confirming that albumin induces transcriptional changes resembling transitional-like B cell signatures.

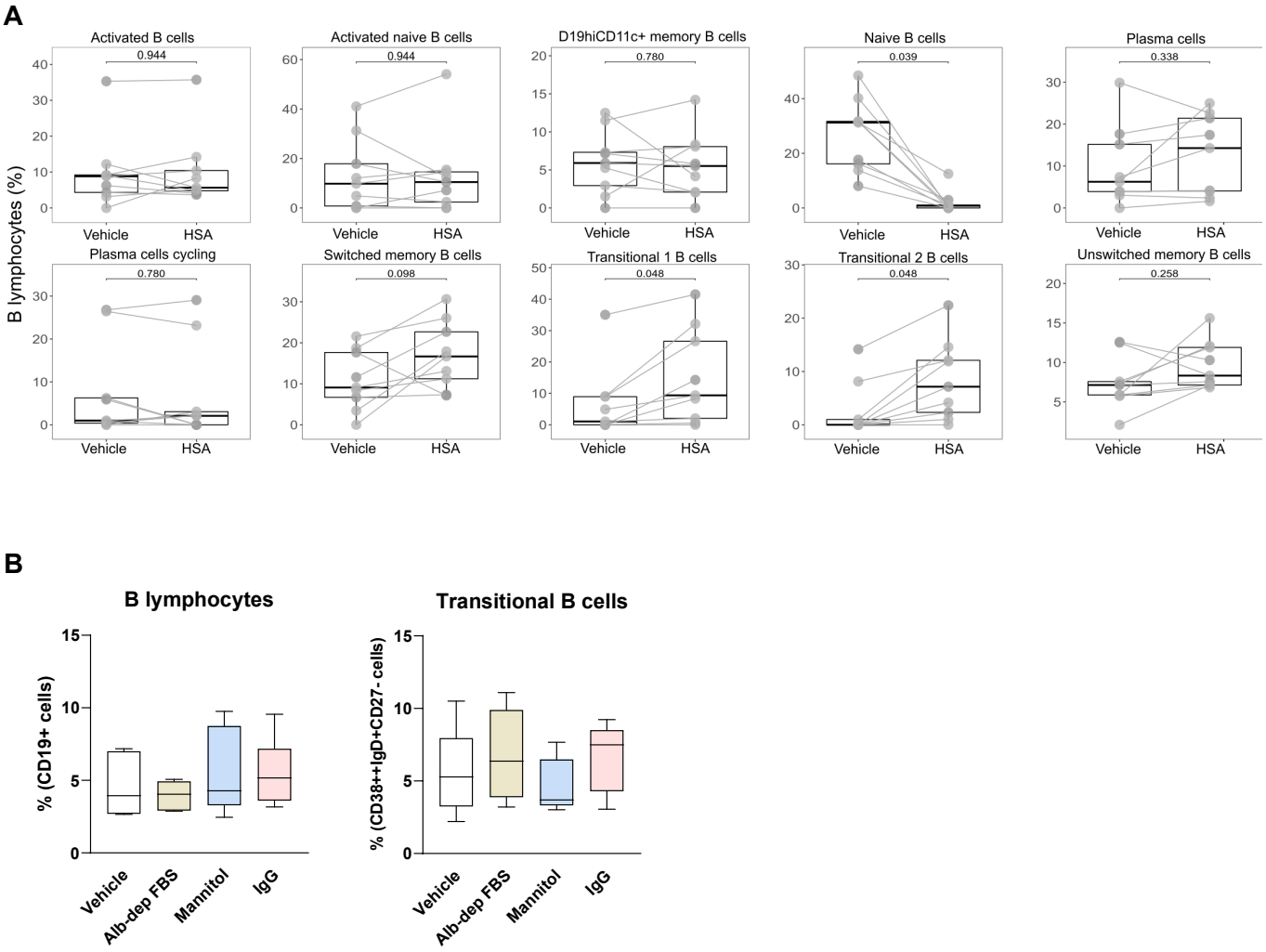

Fig. S5. In vitro effects of human serum albumin (HSA) on B lymphocytes. (A) Boxplots for the abundance of B lymphocyte populations using scRNA-seq data. All comparisons between HSA and vehicle were tested for significance with a paired Wilcoxon signed-rank sum test and adjusted p-values are indicated. This figure has been designed with results obtained in cells from 9 patients with AD cirrhosis. **(B)** Flow cytometry analysis of the B cell and transitional B cell populations in response to vehicle control, 15% albumin-depleted FBS (alb-dep FBS), mannitol (15 mg/ml) and IgG (15 mg/ml).

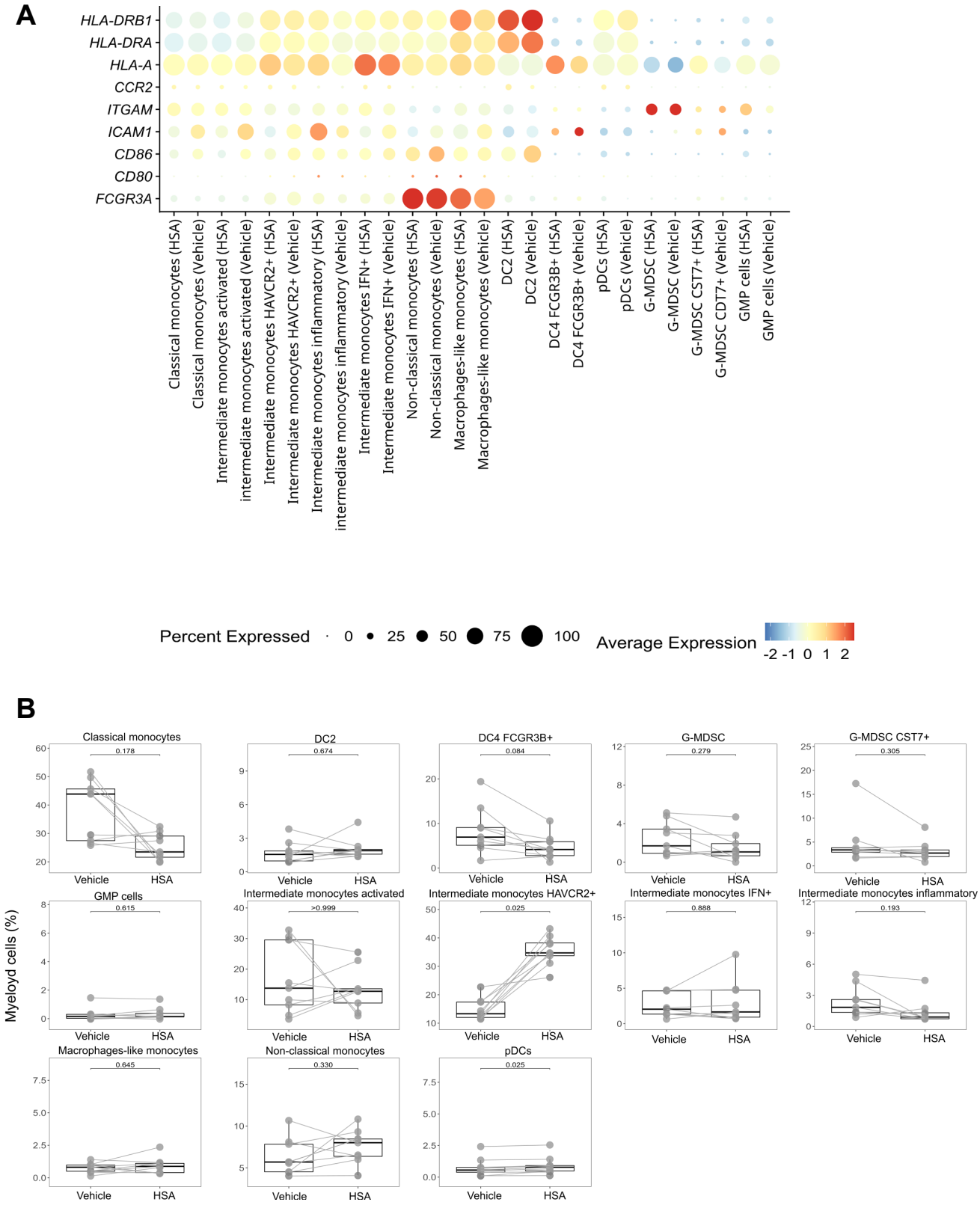

Fig. S6. Effects of HSA on myeloid cells using scRNA-seq. (A) Expression of genes associated with monocyte activation in cells exposed *in vitro* to either vehicle or HSA. **(B)** Boxplots for the abundance of myeloid cells. All comparison of cell type abundance between HSA and vehicle were tested for significance with a paired Wilcoxon signed-rank sum test, and adjusted p-values are indicated. This figure has been designed with results obtained in cells from 9 patients with AD cirrhosis.

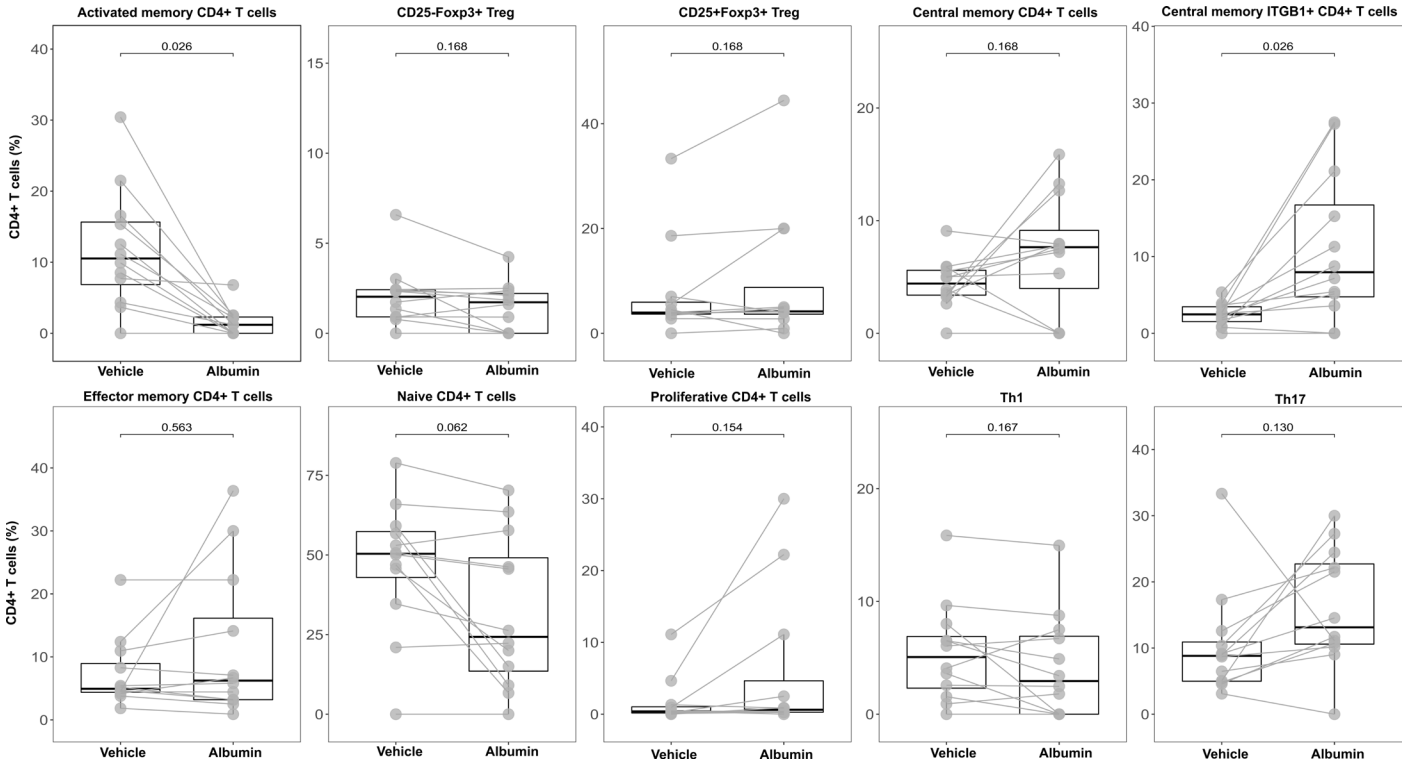

Fig. S7. Analysis of the cell type proportions for patients' CD4$^+$ T cells exposed *in vitro* to albumin. This figure has been designed with results obtained in cells from 9 patients with AD cirrhosis. Boxplots for the abundance of CD4$^+$ T cells. All comparison of cell type abundance between albumin and vehicle were tested for significance with a paired Wilcoxon signed-rank sum test; adjusted P values are indicated.

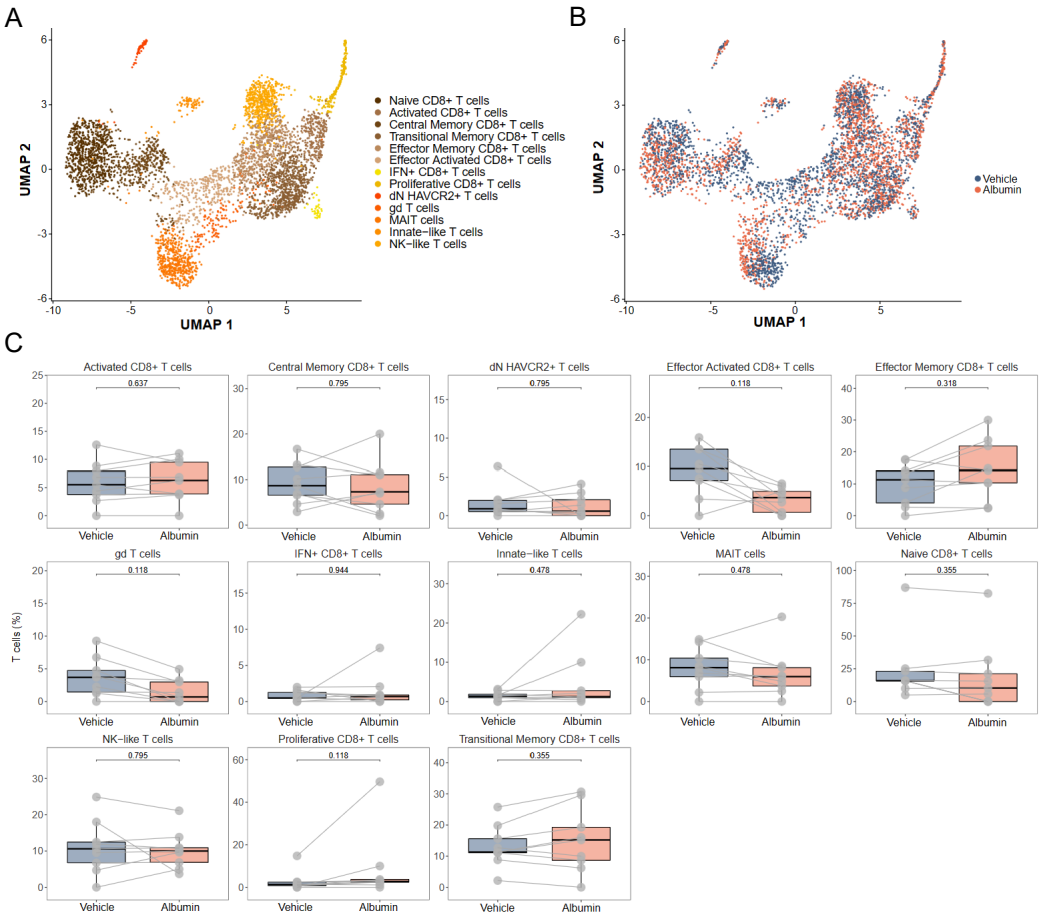

Fig. S8. Analysis of patients' CD8$^+$ and unconventional T cells exposed *in vitro* to albumin. This figure has been designed with results obtained in cells from 9 patients with AD cirrhosis. **(A)** UMAP of 3483 CD8$^+$ T cells and 1292 unconventional T cells exposed to albumin and vehicle, colored by cell populations. **(B)** Overlay of albumin and vehicle exposure on the CD8 and unconventional T-cell UMAP. **(C)** Box plots for the abundance of CD8 and unconventional T cell types after albumin exposure. All comparison of cell type abundance between albumin and vehicle were tested for significance using a paired Wilcoxon signed-rank sum test; adjusted p-values are indicated.

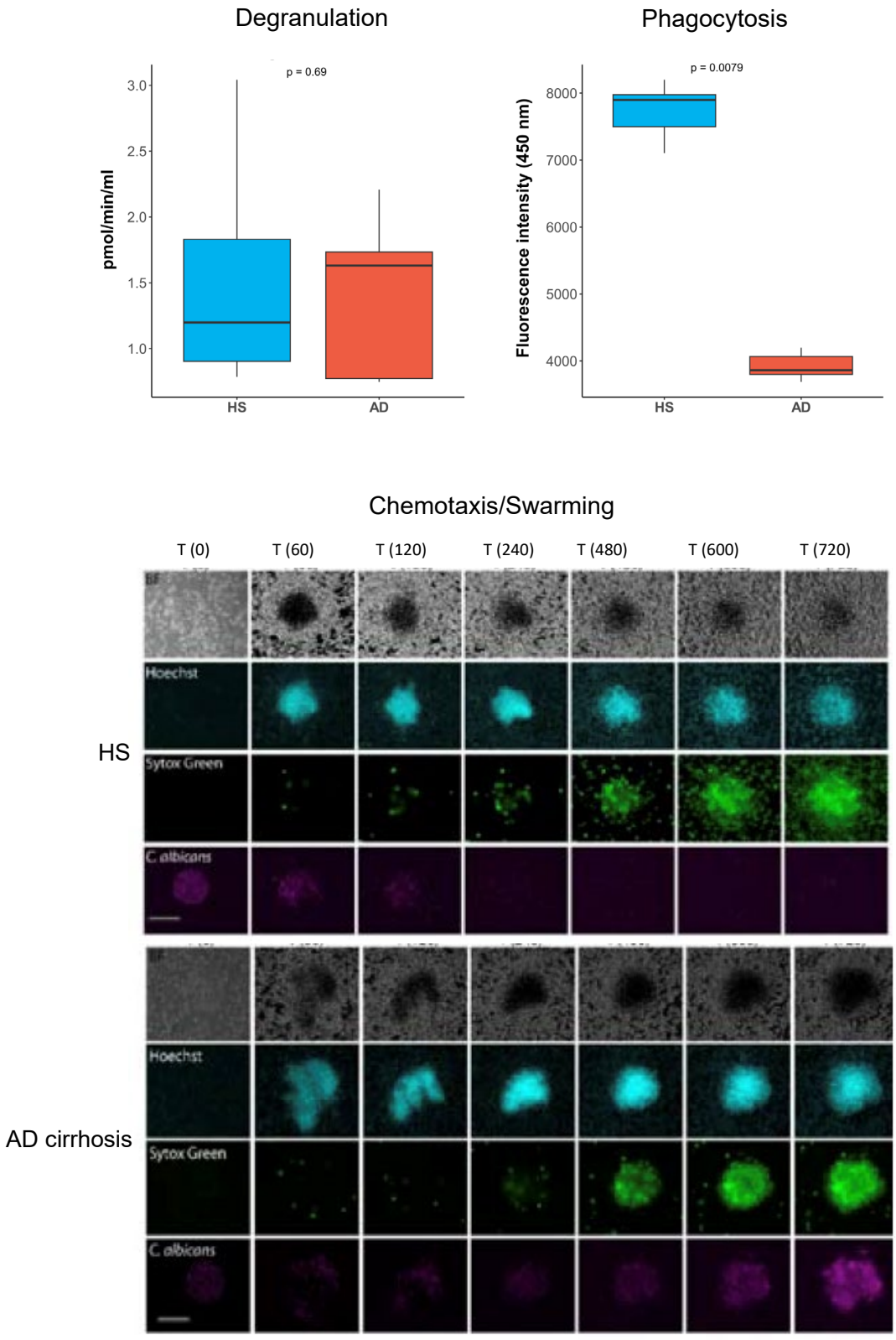

Fig. S9. Neutrophils from patients with AD cirrhosis exhibit impaired anti-microbial functions. Neutrophil degranulation was assessed by measuring the MPO enzymatic activity in the cell supernatants. Phagocytosis was assessed by ingestion of FITC-conjugated zymosan bioparticles. Chemotaxis and swarming were assessed through the ability of neutrophils to delay the escape of *Candida albicans* hyphae from the neutrophil swarm.

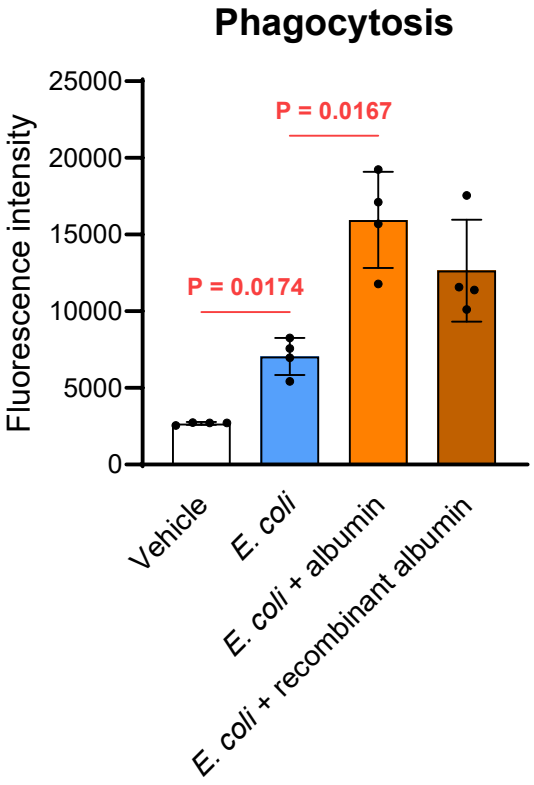

Fig. S10. Phagocytic capacity assessed by incubating neutrophils with fluorescently labeled *E. coli* alone or in the presence of albumin and recombinant albumin for 60 min and compared to vehicle control.

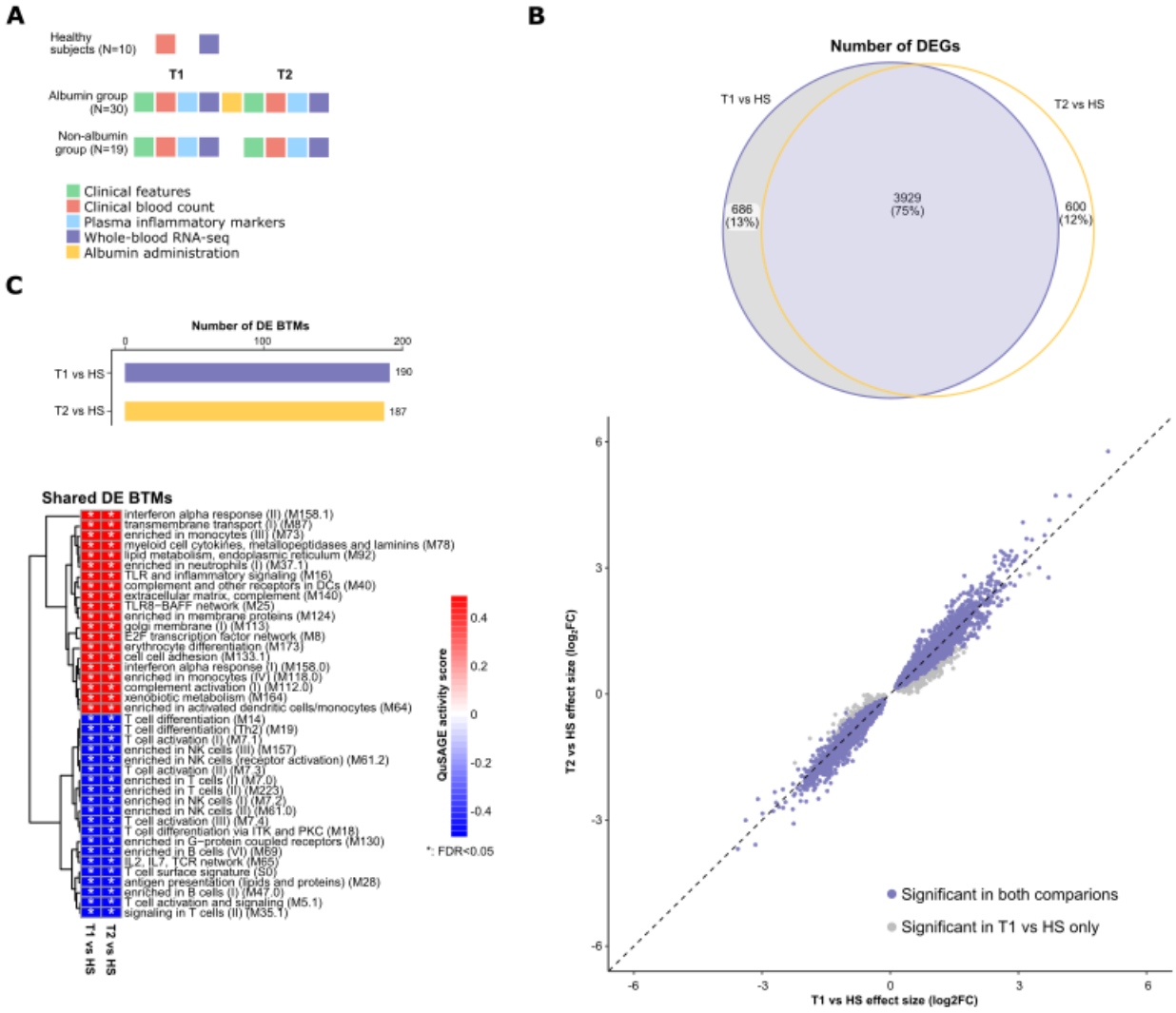

Fig. S11. Whole-blood transcriptional characteristics of all patients at T1 and T2 stages. **(A)** Overview of the longitudinal collection of clinical data and blood specimens (including blood that has been used for RNA-sequencing [RNA-seq]) in 49 patients at time 1 (T1, at enrollment) when they had AD cirrhosis and high risk of developing ACLF and at time 2 (T2) when they had progressed to ACLF. Thirty patients had received intravenous albumin when progressing from T1 to T2. Nineteen patients had not received albumin during the progression to ACLF. Ten age-matched healthy subjects were also studied, but only once. **(B)** Top, Venn diagram showing the overlap of differentially expressed genes (DEGs) in two pairwise comparisons, T1 vs healthy subjects and T2 vs healthy subjects. Bottom, Differential expression effect-size (log2 FC) of T2 compared with T1 changes for the 4615 T1 DEGs. **(C)** Top, number of differentially expressed (DE) blood transcription modules (BTMs) in two pairwise comparisons (T1 vs healthy subjects and T2 vs healthy subjects). Bottom, heatmap showing representative significantly upregulated BTMs and downregulated BTMs that are shared in two comparisons, T1 vs healthy subjects and T2 vs healthy subjects. BTMs are hierarchically clustered based on significant QuSAGE activity scores obtained in the comparison of T1 with healthy subjects. Asterisks denote false-discovery rate (FDR) <0.05. Color represents QuSAGE activity score.

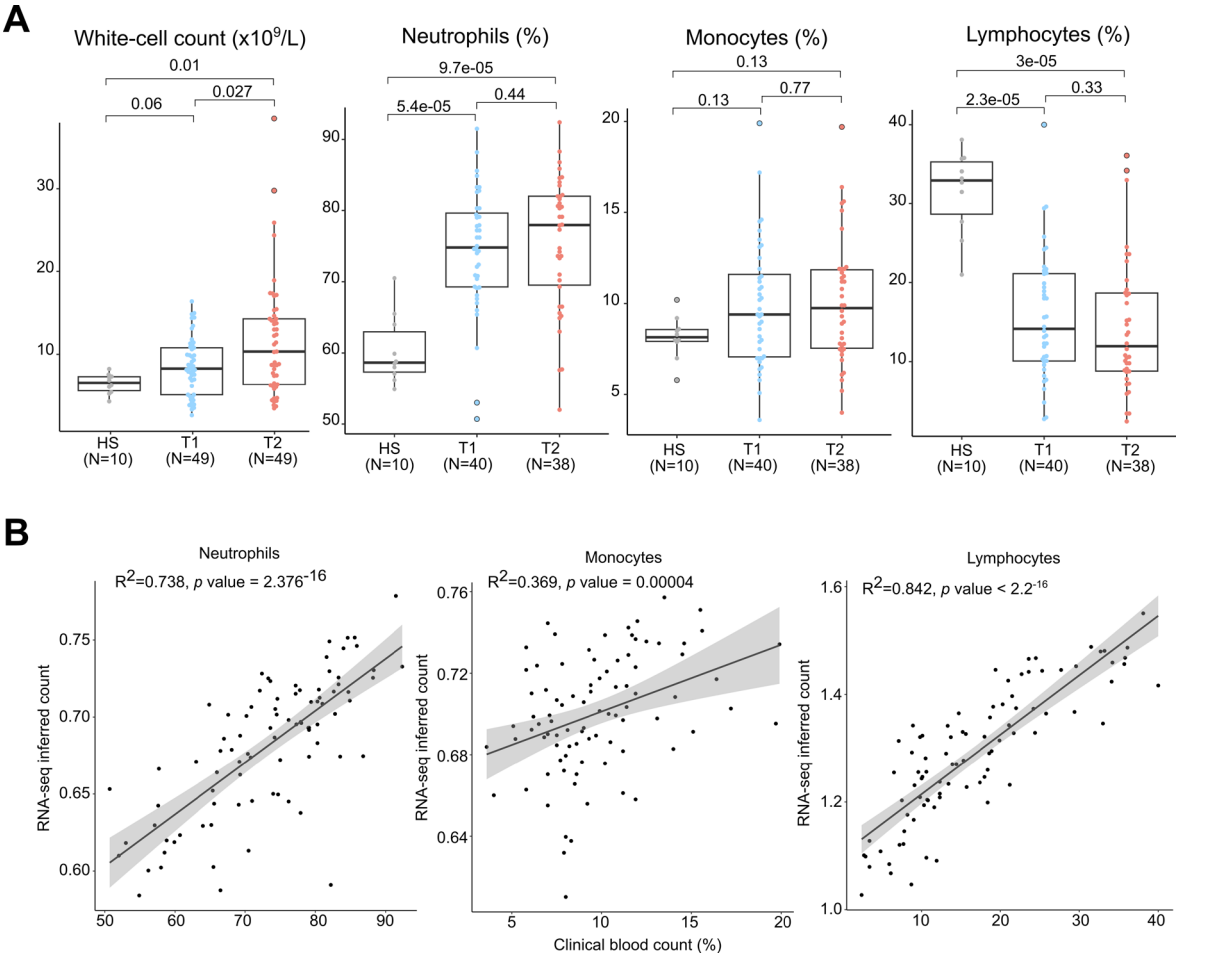

Fig. S12. Clinical blood counts and RNA-seq-inferred blood counts. Longitudinal collection of blood specimens was used for clinical blood count measurements and RNA-sequencing [RNA-seq]) in 49 patients at time 1 (T1, at enrollment) when they had pre-ACLF and at time 2 (T2) when they had progressed to ACLF. Ten age-matched healthy subjects were also studied, but only once. (A) Box plots of clinical complete blood counts were obtained in healthy subjects, and in patients at T1 and T2. There were no missing data in healthy subjects and for white blood cell count in patients. In patients, there were missing data for differential counts of neutrophils, monocytes, and lymphocytes in 2 patients. The horizontal line in each box represents the median, the lower and upper boundaries of the boxes the interquartile range, and the length of the vertical lines are 1.5 times the interquartile range. The P values are from Kruskal–Wallis tests followed by Mann–Whitney U tests. (B) Neutrophil, lymphocyte, and monocyte counts in paired clinical complete blood counts as compared with the RNA-seq-inferred blood counts obtained with the use of peripheral blood (47 paired specimens from healthy subjects, pre-ACLF and ACLF). The shaded areas represent the 95% confidence intervals. To obtain this figure, we correlated the clinical differential blood counts for neutrophils, monocytes and lymphocytes from all study participants including healthy subjects with the corresponding RNA-seq–inferred counts for these white cells (calculated based on the results of the SingleR software of RNA deconvolution for 10 main immune-cell types; see **Fig. S13A**).

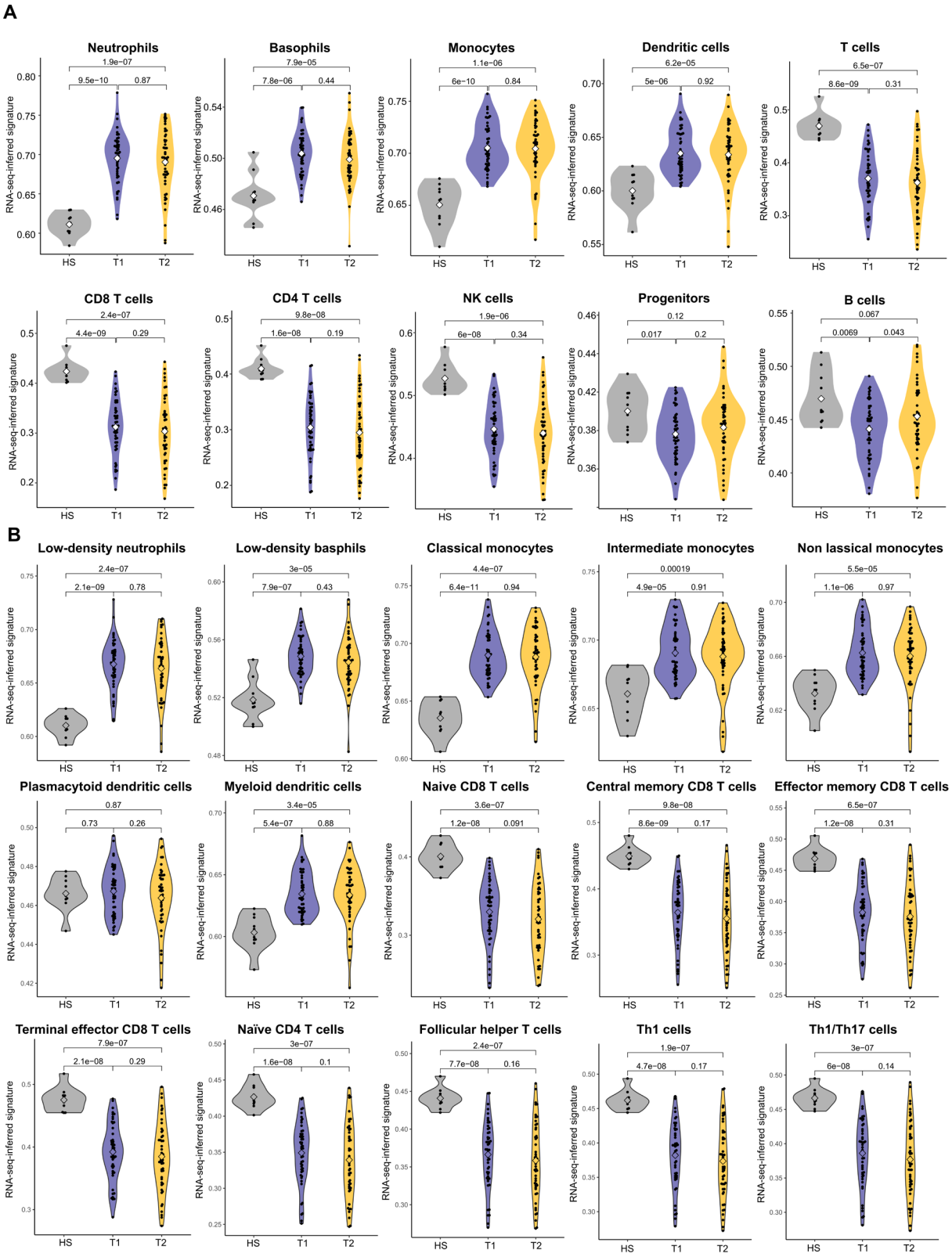

Continued on next page.

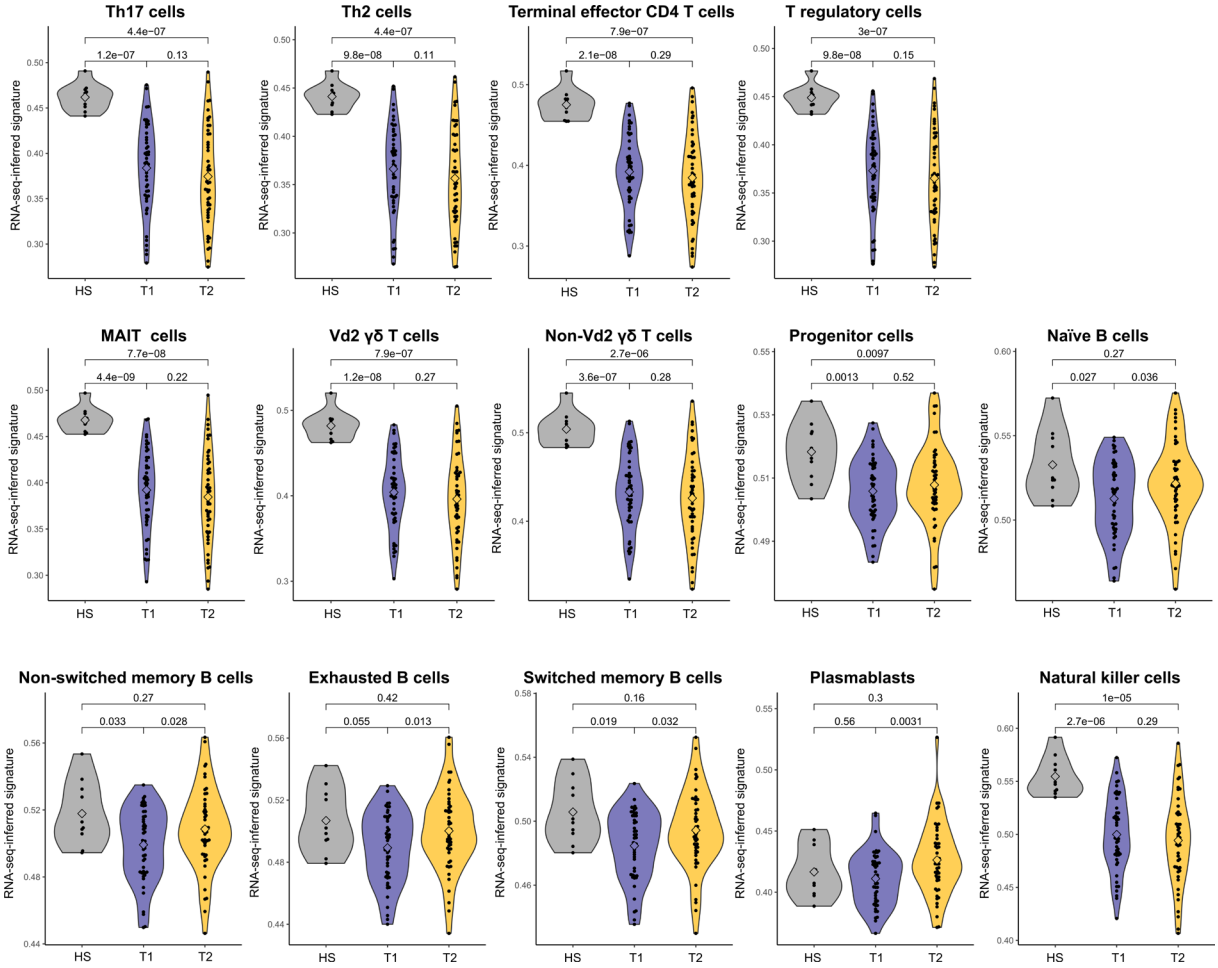

Fig. S13. Violin plots of RNA-seq-inferred signatures of blood immune cells in all patients at T1 and T2 and healthy subjects. Longitudinal collection of blood specimens was used for RNA-sequencing [RNA-seq]) in 49 patients, at time 1 (T1, at enrollment) when they had pre-ACLF, and at time 2 (T2) when they had progressed to ACLF. Ten age-matched healthy subjects were also studied, but only once. Whole-blood RNA-seq data were analyzed with the use of the SingleR software to determine signatures for each of the 10 main immune-cell types **(A)** and each of the 29-fine immune-cell types **(B).** White rhomboid symbols indicate medians. The P values are from Kruskal–Wallis tests followed by Mann–Whitney U tests.

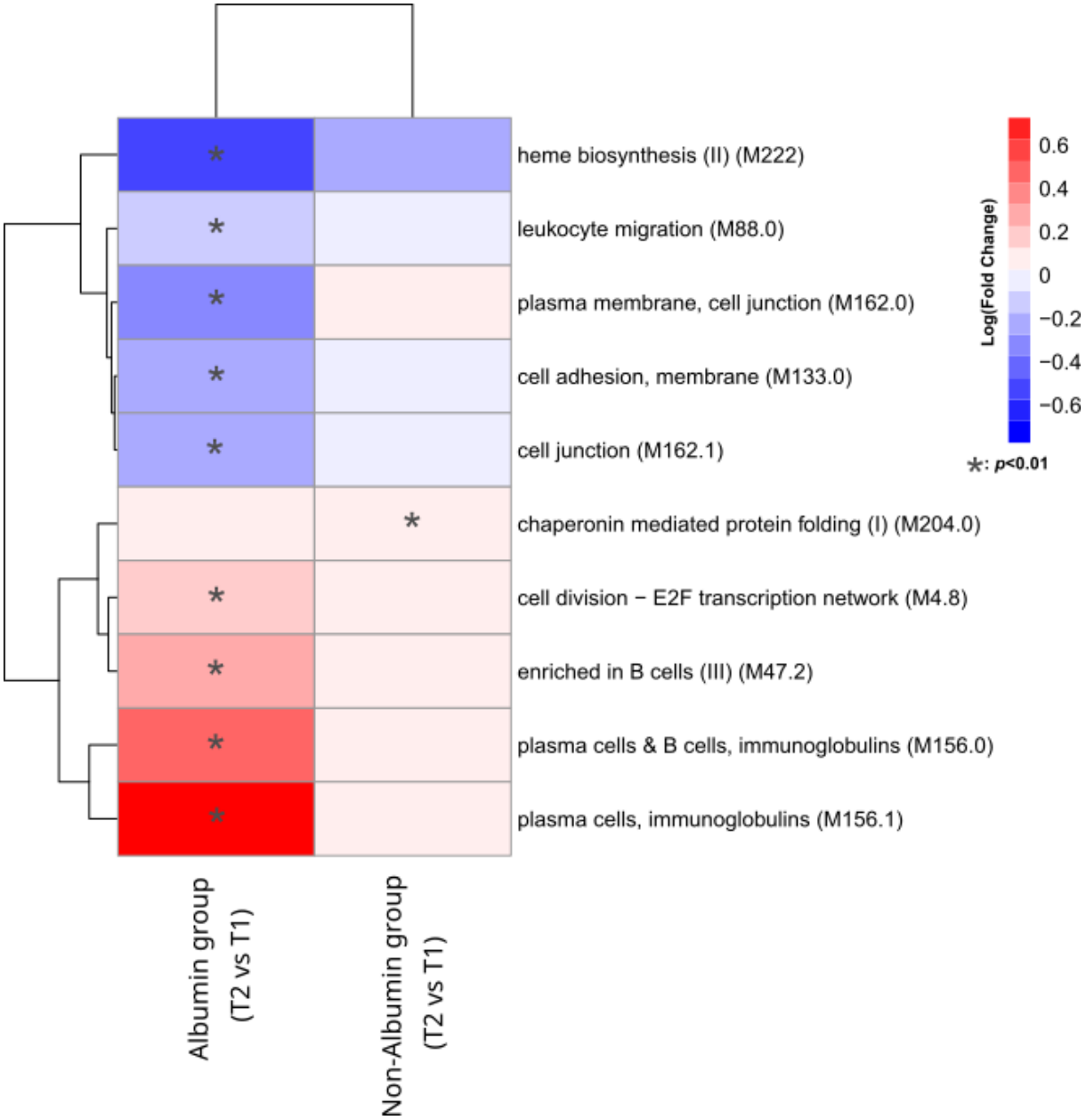

Fig. S14. Analysis of BTMs after adjusting by a non-linear regression multivariate model the transcriptomic data by disease severity of each patient estimated by the MELD score.

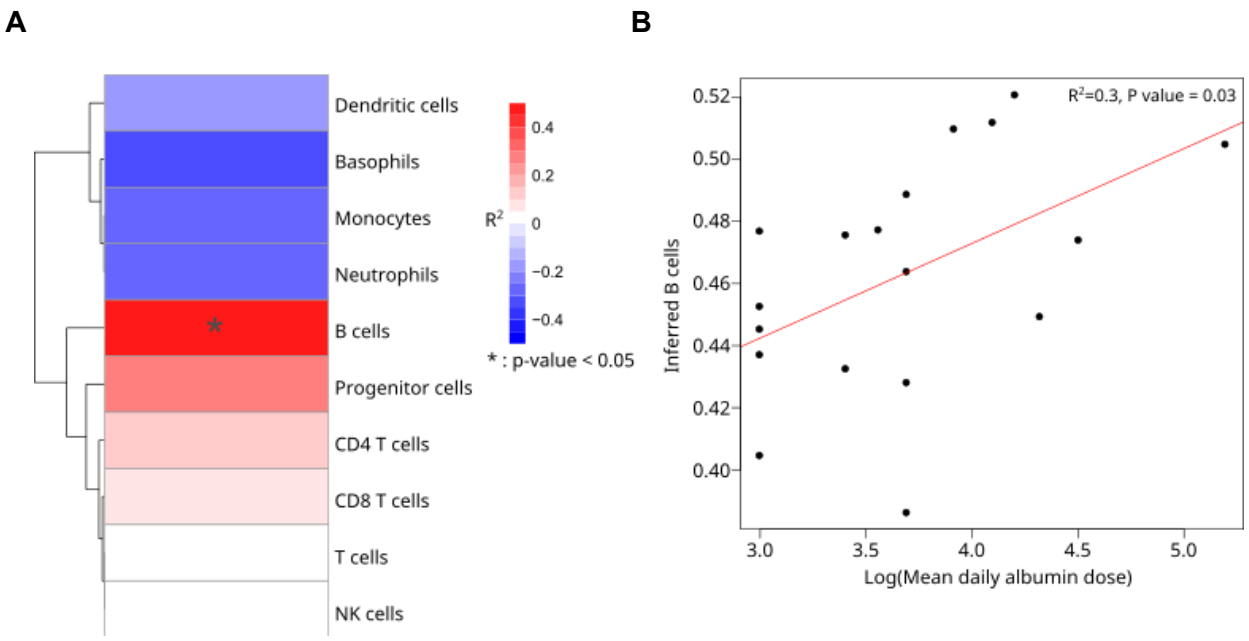

Fig. S15. (A) Correlation between mean daily albumin dose and the number of circulating immune cells inferred from Monaco cell population estimations. **(B)** Correlation between mean daily albumin dose and the number of B cells by means of Monaco estimation.

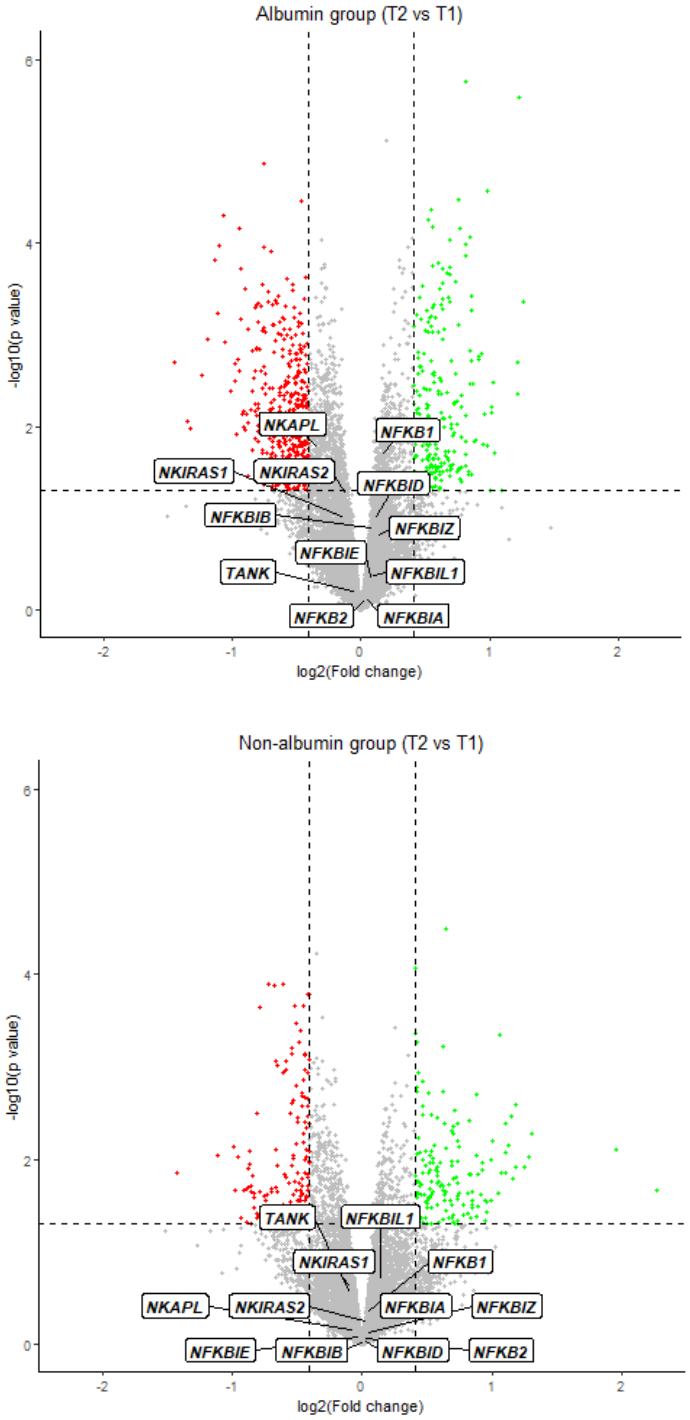

Fig. S16. Volcano plots showing differential expression effect-size (log2 FC) in genes of the NF-κB family between T2 and T1 plotted against significance (-log10 p value), for the albumin group (top) and non-albumin group (bottom). In both volcano plots, gray points indicate genes with no significant difference in expression between T2 and T1 (with absolute FC of less than 1.5 and P>0.05, i.e., -log10 P <1.3). *NFKB1,* Nuclear Factor Kappa B Subunit 1; *NFKB2,* Nuclear Factor Kappa B Subunit 2; *NKAPL*: NFKB Activating Protein Like, *NKAP,* NFKB Activating Protein; *TANK*, TRAF Family Member Associated NFKB Activator; *NKRF*, NFKB Repressing Factor; *NFKBIA*, NFKB Inhibitor Alpha; *NFKBIB*, NFKB Inhibitor Beta; *NFKBIZ*, NFKB Inhibitor Zeta; *NFKBID*, NFKB Inhibitor Delta; *NFKBIE*, NFKB Inhibitor Epsilon; *NFKBIL1*, NFKB Inhibitor Like 1; *NKIRAS1*, NFKB Inhibitor Interacting Ras Like 1; *NKIRAS2* ,NFKB Inhibitor Interacting Ras Like 2.

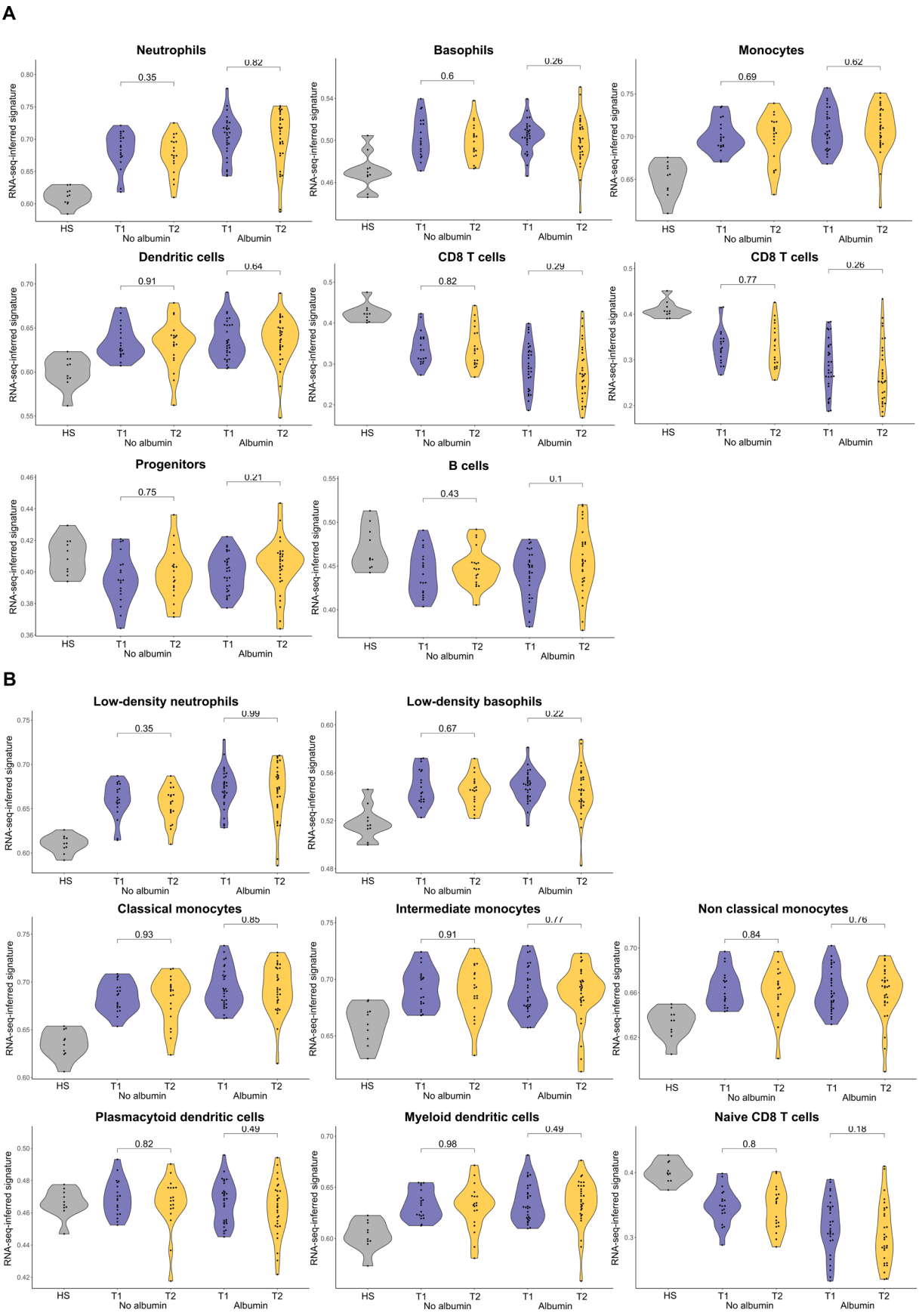

Continued on next page.

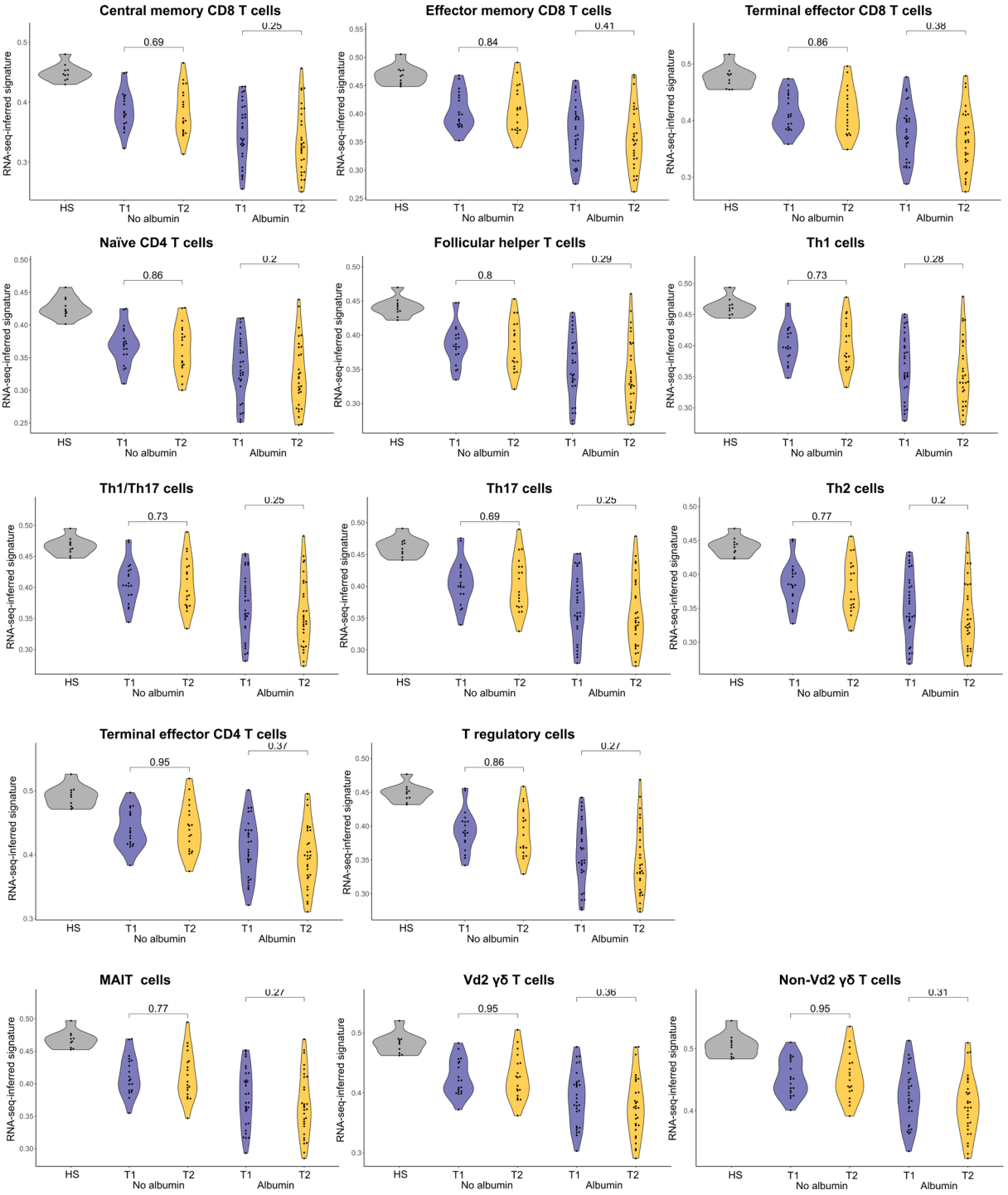

Continued on next page.

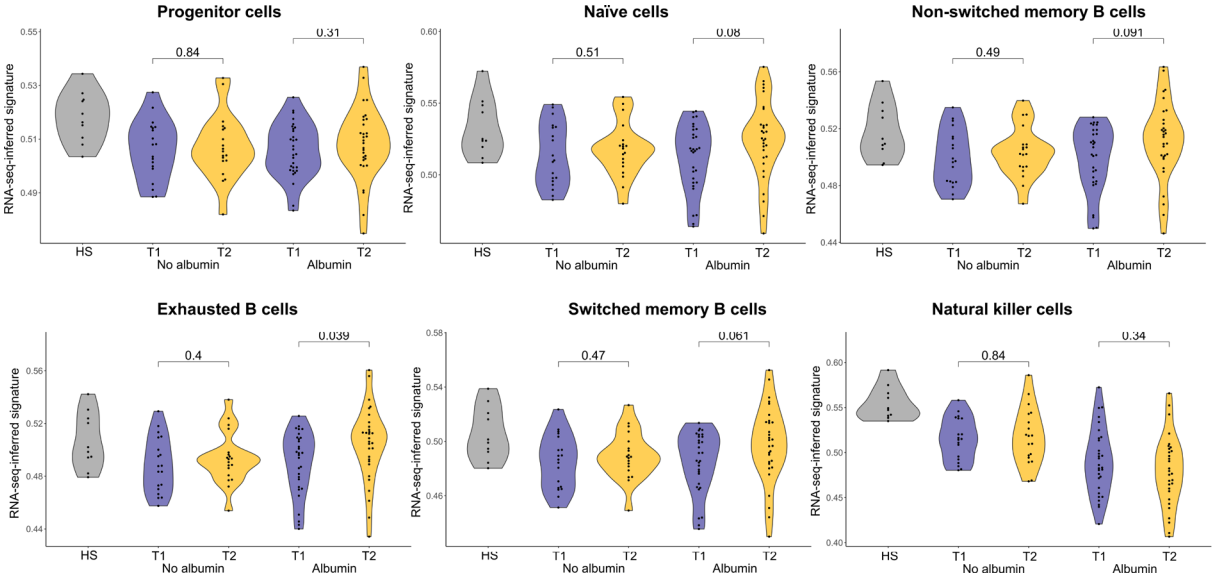

Fig. S17. Violin plots of RNA-seq-inferred signatures of blood immune cells at T1 and T2 in patients of the albumin group and those of the non-albumin group. Longitudinal collection of blood specimens was used for RNA-sequencing [RNA-seq]) in 49 patients at time 1 (T1, at enrollment) when they had pre-ACLF and at time 2 (T2) when they had progressed to ACLF. Thirty patients had received intravenous albumin when progressing from T1 to T2. Nineteen patients had not received albumin during the progression to ACLF. Whole-blood RNA-seq data were analyzed with the use of the SingleR software to determine signatures for each of the 10 main immune-cell types **(A)** and each of the 29-fine immune-cell types **(B).** Of note, results of plasmablasts are not shown in panel B because these results are shown in Figure 5D, top. Results obtained in 10 healthy subjects are provided for reference. The P values are from Kruskal–Wallis tests followed by Mann–Whitney U tests.

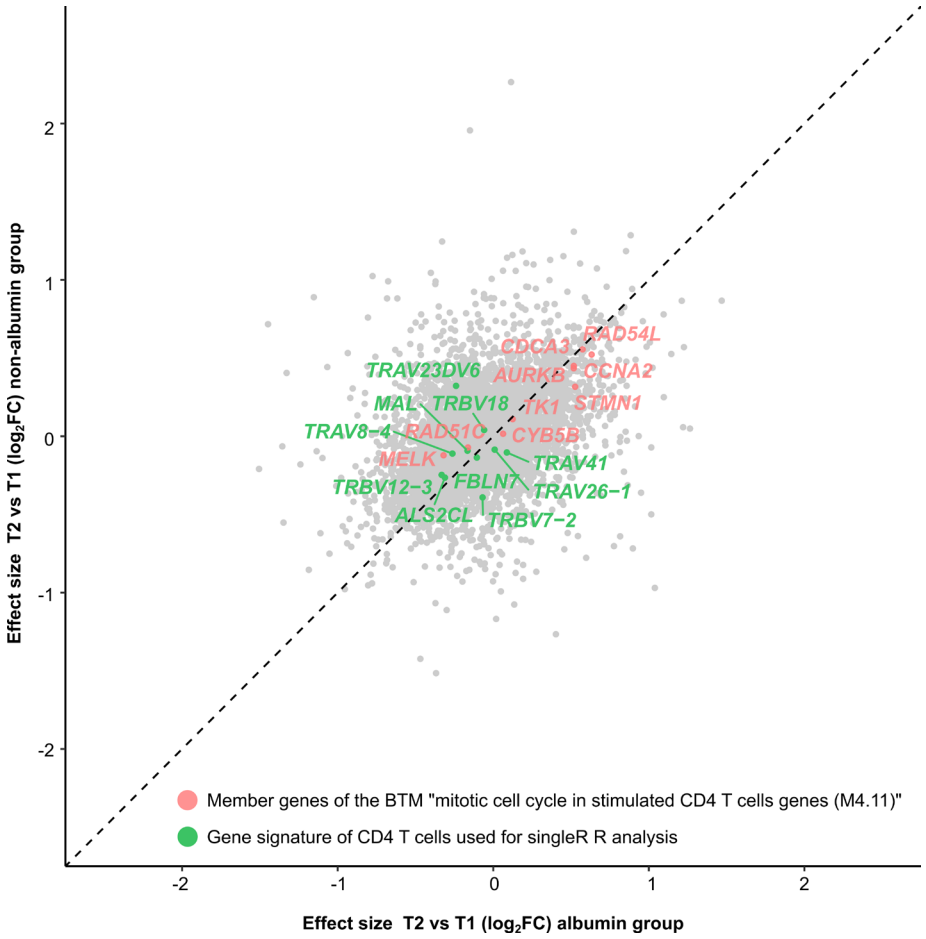

Fig. S18. Scatter plots showing the lack of overlap between member genes for the BTM related to mitotic cell cycle in stimulated CD4 T cells (M4.11) and genes defining the signature CD4 T cells used in the SingleR pipeline. There were 9 genes (red color) and 10 genes (green color), respectively.

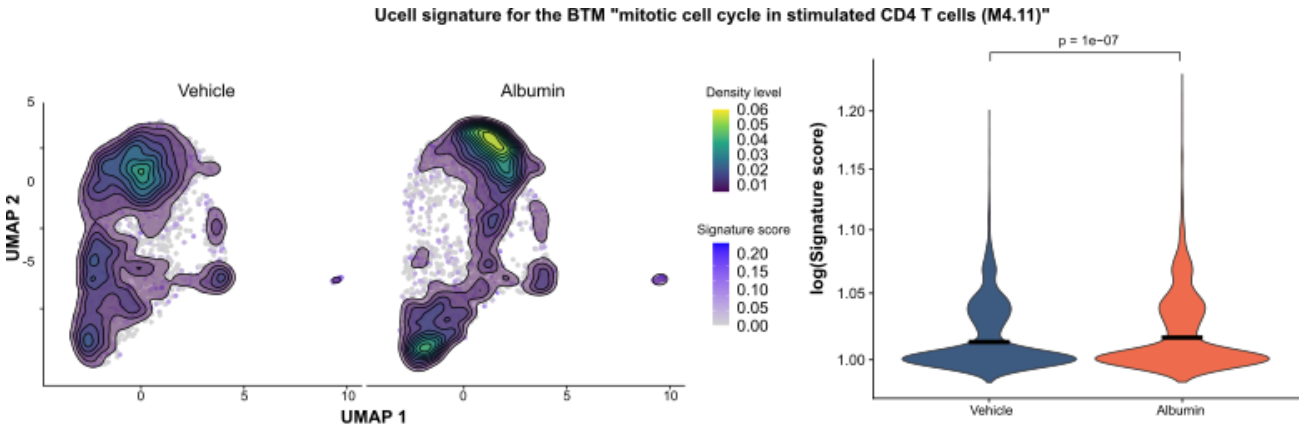

Fig. S19. Left, representative density plot showing the signature score for the BTM "mitotic cell cycle in stimulated CD4 T cells (M4.11)" on the CD4 T cells UMAP across vehicle and albumin conditions. Right, comparison of log(signature score) for the BTM 4.11 between albumin and vehicle on the CD4 T cell compartment. Statistical analysis for BTM signature was performed using a Wilcoxon signed-rank sum test; p-value significance is indicated. All comparison of cell type abundance between albumin and vehicle were tested for significance by paired Wilcoxon signed-rank sum test, and significant adjusted p-values are indicated.

Supplementary tables

Table S1. Characteristics of the thirty-four healthy volunteers and twenty patients with AD cirrhosis from whom PBMCs were isolated for *in vitro* experiments.

Characteristics	Healthy volunteers	Patients with AD cirrhosis
Demographic feature		
Age – yr	48.6±13.5	57.4±4.5
Male sex – no. (%)	17 (50)	15 (75)
Markers of organ function		
MELD score[†]	NA	22.3±8.8
CLIF-C OF score[‡]	NA	9±3.6
Organ system failure – no. (%)[§]	NA	
Liver failure	-	8 (40)
Kidney failure	-	6 (30)
Cerebral failure	-	3 (15)
Coagulation failure	-	7 (35)
Circulatory failure	-	12 (60)
Respiratory failure	-	0 (0)
ACLF grade – no. (%)	NA	
Grade 1	-	7 (35)
Grade 2-3	-	3 (15)
Precipitating events		
Infection – no. (%)	NA	6 (30)
Alcoholic hepatitis – no. (%)	NA	7 (35)
Laboratory data		
INR – median (IQR)	1.0 (0.9-1.0)	1.9 (1.5-2.4)*
Median total bilirubin (IQR) – mg/dL	0.6 (0.5-0.9)	4.9 (2-15.1)*
Median serum creatinine (IQR) – mg/dL	0.9 (0.7-1.0)	1.9 (1-2.3)*
Serum sodium – mmol/L	141.4±2.4	132.8±2.2*
Median serum albumin (IQR) – g/dL	4.6 (4.1-4.8)	2.8 (2.6-3.3)*
Median white-cell count (IQR) – $x10^3/mm^3$	6.4 (5.3-7.3)	6.6 (5.7-8.7)*
Median differential neutrophil count (IQR) – %	53.1 (46.0-60.5)	73 (65.0-79.0)*
Median differential lymphocyte count (IQR) – %	33.0 (28.4-41.8)	11 (5.4-19.2)*
Median differential monocyte count (IQR) – %	6.4 (5.4-7.8)	4.2 (0.2-7.7)*
Median blood C-reactive protein levels (IQR) – mg/L	0.1 (0.1-0.1)	3.2 (1.9-3.9)*

*Denotes statistical significance differences.

Plus–minus values are mean±SD.

MELD Model for End-Stage Liver Disease, CLIF-C Chronic Liver Failure Consortium, OF organ failure, INR International Normalized Ratio, IQR interquartile range.

Table S2. Characteristics of the nine healthy volunteers and six patients with AD cirrhosis from whom blood neutrophils were isolated for *in vitro* experiments.

Characteristics	Healthy volunteers	Patients with AD cirrhosis
Demographic feature		
Age – yr	49.9±10.7	61.3±9.9
Male sex – no. (%)	4 (55.6)	4 (66)
Markers of organ function		
MELD score†	NA	15.0±4.0
CLIF-C OF score‡	NA	5.3±0.8
Organ system failure – no. (%)§	NA	
Liver failure	-	0 (0)
Kidney failure	-	0 (0)
Cerebral failure	-	0 (0)
Coagulation failure	-	1 (17)
Circulatory failure	-	0 (0)
Respiratory failure	-	0 (0)
ACLF grade – no. (%)	NA	
Grade 1	-	0 (0)
Grade 2-3	-	0 (0)
Precipitating events		
Infection as pre-ACLF/ACLF precipitant – no. (%)	NA	0 (0)
Alcoholic hepatitis as pre-ACLF/ACLF precipitant – no. (%)	NA	0 (0)
Laboratory data		
INR – median (IQR)	1.0 (0.9-1.0)	1.3 (1.3-1.4)
Median total bilirubin (IQR) – mg/dL	0.8 (0.6-0.9)	1.9 (1.3-2.6)*
Median serum creatinine (IQR) – mg/dL	1.0 (0.9-1.1)	1.0 (0.8-1.2)
Serum sodium – mmol/L	141.6±1.3	134.8±4.2*
Median serum albumin (IQR) – g/dL	4.4 (4.2-4.6)	3.3 (2.8-3.6)*
Median white-cell count (IQR) – $x10^3/mm^3$	6.7 (4.0-7.0)	4.2 (3.1-5.4)
Median differential neutrophil count (IQR) – %	51.9 (45.3-62.1)	61.2 (56.5-71.8)*
Median differential lymphocyte count (IQR) – %	31.5 (26.4-44.6)	13.7 (6.0-23.9)*
Median differential monocyte count (IQR) – %	5.7 (5.0-6.6)	8.0 (2.5-9.6)
Median blood C-reactive protein levels (IQR) – mg/L	0.1 (0.1-0.1)	2.4 (1.8-3.0)*

*Denotes statistical significance differences.

Plus–minus values are mean±SD.

MELD Model for End-Stage Liver Disease, CLIF-C Chronic Liver Failure Consortium, OF organ failure, INR International Normalized Ratio, IQR interquartile range.

Table S3. Characteristics of the 49 Patients Enrolled in the HSA Infusion Study at T1 and T2 stages.

Characteristic*			P value
	T1	**T2**	
Age – yr	60.2±9.1[a]		
Male sex – no. (%)	33 (70)		
Markers of organ function			
MELD score	19.1±5.4	25.9±7.0	<0.01
CLIF-C OF score	7.1±1.1	9.9±2.4	<0.01
Organ system failure – no. (%)			
Liver failure	10 (20)	13 (27)	0.63
Kidney failure	0 (0)	36 (73)	<0.01
Circulatory failure	0 (0)	10 (20)	<0.01
Cerebral failure	1 (2)	7 (14)	0.07
Coagulation failure	0 (0)	8 (17)	0.01
Respiratory failure	0 (0)	9 (18)	0.01
ACLF grade – no. (%)			
Grade 1	0 (0)	27 (55)	<0.01
Grade 2-3	0 (0)	22 (45)	<0.01
Precipitating events			
Infection as precipitant at T1 or T2 – n (*%*)	17 (35)	24 (49)	0.22
Alcohol-related hepatitis as precipitant at T1 or T2 – n (*%*)	15 (31)	14 (29)	1
Laboratory data			
INR – median (IQR)	1.5 (1.2-1.7)	1.6 (1.4-2.1)	0.08
Median total bilirubin (IQR) – mg/L	3.5 (1.5-9.9)	3.9 (1.3-13.3)	0.86
Median serum creatinine (IQR) – mg/dL	1.3 (1.1-1.6)	2.3 (1.8-3.0)	<0.01
Serum sodium – mmol/L	132.4±6.3	133.0±-7.7	0.66
Median serum albumin (IQR) – g/dl	2.7 (2.3-3.3)	3.0 (2.6-3.4)	0.15
Median white-cell count (IQR) – $x10^3/mm^3$	7.7 (4.7-10.1)	9.7 (5.9-13.4)	0.03
Median absolute lymphocyte count (IQR) – $x10^3/mm^3$	1.0 (0.6-1.3)	1.1 (0.8-1.7)	0.19
Median absolute monocyte count (IQR) – $x10^3/mm^3$	0.7 (0.4-1.0)	0.9 (0.6-1.2)	0.13
Median absolute neutrophil count (IQR) – $x10^3/mm^3$	5.7 (3.5-7.4)	6.8 (3.9-10.3)	0.15
Median C-reactive protein (IQR) – *mg/L*	24.5 (11.2-42.8)	25.8 (13.4-65.8)	0.47
Median blood levels of protein mediators of inflammation (IQR) – pg/ml			
Eotaxin	70.2 (43.1-105.6)	80.2 (56.4-118.7)	0.19
G-CSF	20.1 (5.6-58.6)	21.7 (6.1-75.1)	0.84
Interferon-α2	11.3 (2.9-23.1)	16.8 (5.4-27.9)	0.30
Interferon-γ	26.2 (6.4-86.6)	25.2 (9.3-64.7)	0.81
Interleukin-1α	3.0 (1.3-5.7)	2.0 (0.7-4.7)	0.25
Interleukin-1β	5.4 (2.7-10.3)	5.2 (2.0-10.3)	0.93
Interleukin-6	17.0 (7.9-39.7)	27.1 (10.6-71.5)	0.07
Interleukin-8	4.9 (2.8-10.9)	5.8 (2.8-16.7)	0.57

Interleukin-10	6.1 (1.5-23.4)	5.8 (3.5-20.0)	0.43
IP-10 (CXCL10)	214 (131-376)	234 (148-540)	0.46
MIP-1α (CCL3)	11.4 (4.6-22.5)	14.1 (6.7-25.2)	0.28
MIP-1β (CCL4)	15.7 (11.8-20.7)	17.0 (12.7-28.7)	0.27
Tumor necrosis factor α	32.4 (17.9-43.6)	35.4 (21.8-60.3)	0.44
VEGF	4.4 (1.0-9.5)	7.6 (2.9-14.2)	0.09
Deaths – n (%)			
By 28 days	9 (18)		
By 90 days	23 (47)		

*Plus–minus values are mean±SD.

To convert the values for serum creatinine to micromoles per liter, multiply by 88.4. To convert the values for bilirubin to micromoles per liter, multiply by 17.1. Normal values for blood inflammatory mediators are shown in **Table S4**. MELD Model for End-Stage Liver Disease, CLIF-C Chronic Liver Failure Consortium, OF organ failure, INR International Normalized Ratio, IQR interquartile range, G-CSF granulocyte-colony stimulating factor, IP-10 interferon-inducible protein 10, CXCL C-X-C motif chemokine ligand, MCP-1 monocyte chemoattractant protein 1, CCL CC motif chemokine ligand, MIP macrophage inflammatory protein, and VEGF vascular endothelial growth factor.

Table S4. Plasma Levels (pg/ml) of Inflammatory Mediators in 78 Healthy Subjects.

Mediator	Median value (IQR)*
Eotaxin	41.2 (31.7-56.1)
G-CSF	5.6 (2.7-8.2)
IFN-α2	19.1 (10.8-37.2)
IFN-γ	15.2 (6.2-24.3)
Interleukin-1α	1.8 (0.7-4.7)
Interleukin-1β	2.6 (1.2-6.3)
Interleukin-6	0.4 (0.2-0.7)
Interleukin-8	0.3 (0.2-0.6)
Interleukin-10	2 (0.8-3.8)
IP-10 (CXCL10)	74.4 (55.3-103)
MIP-1α (CCL3)	7.6 (3.4-13.8)
MIP-1β (CCL4)	8.1 (6.5-10.1)
Tumor necrosis factor α	8.8 (6.1-14.5)
VEGF	6.3 (2.5-16.2)

*IQR denotes interquartile range, G-CSF granulocyte-colony stimulating factor, IP-10 interferon-inducible protein 10, CXCL C-X-C motif chemokine ligand, MCP-1 monocyte chemoattractant protein 1, CCL CC motif chemokine ligand, MIP macrophage inflammatory protein, and VEGF vascular endothelial growth factor.

Table S5 is provided as a separate .xls file. This table shows the results of enrichment analyses of the blood transcription module (BTM) space with the use of QuSAGE.

Supplementary video legend

The dynamics of neutrophil recruitment and candida growth. *Top left:* *Candida* only in microfluidic chambers. *Top right:* Neutrophils only in microfluidic chambers in the presence of LTB_4 (100 nM). *Bottom left:* Neutrophils recruited in the presence of albumin are more likely to swarm and contain any *Candida* growing in hyphae after phagocytosis. Neutrophil swarming appears to be attracting more neutrophils from outside the chambers. *Bottom right:* Neutrophils recruited in vehicle-control conditions phagocytose the yeast but are less likely to control the growth of *Candida* that escape the initial control and grown into hyphae. Fewer neutrophils are recruited after the neutrophils encounter *Candida* hyphae.

Supplementary references

1. Trebicka J, Fernandez J, Papp M, et al. The PREDICT study uncovers three clinical courses of acutely decompensated cirrhosis that have distinct pathophysiology. J Hepatol 2020;73:842-54.
2. Moreau R, Jalan R, Ginès P, et al. Acute-on-chronic liver failure is a distinct syndrome that develops in patients with acute decompensation of cirrhosis. Gastroenterology 2013;144:1426-37.
3. Arroyo V, Moreau R, Jalan R. Acute-on-Chronic Liver Failure. N Engl J Med 2020;382:2137-45.
4. Clària J, Stauber RE, Coenraad MJ, et al. Systemic inflammation in decompensated cirrhosis: characterization and role in acute-on-chronic liver failure. Hepatology 2016;64:1249-64.
5. Weiss E, de la Grange P, Defaye M, et al. Characterization of Blood Immune Cells in Patients With Decompensated Cirrhosis Including ACLF. Front Immunol 2021;11:619039.
6. Hao Y, Hao S, Andersen-Nissen E, et al. Integrated analysis of multimodal single-cell data. Cell 2021;184:3573-3587.
7. Stoeckius M, Zheng S, Houck-Loomis B, et al. Cell Hashing with barcoded antibodies enables multiplexing and doublet detection for single cell genomics. Genome Biol. 2018;19: 224.
8. Luecken MD, Theis FJ. Current best practices in single-cell RNA-seq analysis: a tutorial. Mol Syst Biol. 2019;15:e8746.
9. Korsunsky I, Millard N, Fan J, et al. Fast, sensitive and accurate integration of single-cell data with Harmony. Nat Methods. 2019;16:1289-1296.
10. Andreatta M, Carmona SJ. UCell: Robust and scalable single-cell gene signature scoring. Comput Struct Biotechnol J. 2021;19:3796-3798.

11. Frankish A, Diekhans M, Ferreira AM, et al. GENCODE reference annotation for the human and mouse genomes. Nucleic Acids Res. 2019;47:D766-D773.
12. Ritchie ME, Phipson B, Wu D, et al. Limma powers differential expression analyses for RNA-sequencing and microarray studies. Nucleic Acids Res. 2015;43:e47.
13. Yaari G, Bolen CR, Thakar J, et al. Quantitative set analysis for gene expression: a method to quantify gene set differential expression including gene-gene correlations. Nucleic Acids Res. 2013;**41**:e170.
14. Hagan T, Gerritsen B, Tomalin LE, et al. Transcriptional atlas of the human immune response to 13 vaccines reveals a common predictor of vaccine-induced antibody responses. Nat Immunol. 2022;23:1788-1798.
15. Aran AP, Looney AP, Liu L, et al. Bhattacharya. Reference-based analysis of lung single-cell sequencing reveals a transitional profibrotic macrophage. Nat Immunol. 2019;20:163-172.
16. Monaco G, Lee V, Xu W, et al. RNA-Seq Signatures normalized by mRNA abundance allow absolute deconvolution of human immune cell types. Cell Rep. 2019;26:1627-1640.
17. Ellett F, Jalali F, Marand AL, et al. Microfluidic arenas for war games between neutrophils and microbes. Lab Chip. 2019;19:1205-1216.
18. Stewart A, Ng JC, Wallis G, et al. Single-Cell Transcriptomic Analyses Define Distinct Peripheral B Cell Subsets and Discrete Development Pathways. Front Immunol. 2021;12:602539.